Космични изследвания в България

Том 5 . София . 1986

Българска академия на науките

Address .

Space Research in Bulgaria
Central Laboratory for Space Research
Bulgaria, 1000 Sofia, 1 Rouski Bld.

Адрес

Космични изследвания в България
Централна лаборатория по космични изследвания
1000 София, бул. „Руски“ № 1

629.13 (05)

Издателство на Българската академия на науките

Редактор *Л. Шведова* Коректор *Е. Тошева* Техн. редактор *Ал. Иванов*
Изд. индекс 10219 Дадена за набор на 7. VIII. 1985 г. Подп. за печат на 24. I. 1986 г. Код 28—9532422211
70×1000/16 Тираж 700 Печ. коли 4,25 Изд. коли 5,50 УИК 5,58 Цена 0,95 лв. 2332-6-85
Печатница на БАН — 1113 София, ул. „Акад. Георги Бончев“ Пор. 400

ISSN 0204-9104

Space Research in Bulgaria

Volume 5. Sofia. 1986

Bulgarian Academy of Sciences

Contents

Содержание

BULGARIAN ACADEMY OF SCIENCES

SPACE RESEARCH IN BULGARIA, 5

Sofia . 1986

Academician Prof. Dr Kiril Borisov Serafimov

Born on May 24th, 1932 in Sofia. Married, with three children. Graduate of the Mechano-Technical Secondary School of Sofia in 1951 as the top student of his alumnus. Graduated from the V. I. Lenin Higher Mechanical and Electrical Engineering Institute as an outstanding student in radio engineering.

In 1957 he became Research Fellow at the Scientific Research Institute of Communications (NIIS). There he initiated the establishment of ionospheric stations and multiple technical developments. He was trained in the field of ionospheric research at the Soviet Institute for Earth Magnetism, Ionosphere and Radiowave Propagation in 1958. Since the beginning of 1961 worked in the Geophysical Institute of the Bulgarian Academy of Sciences. In 1964 became Candidate of the Physico-Mathematical Sciences at the Lomonosov State University of Moscow. In 1969 defended a thesis and became Doctor of the Physico-Mathematical Sciences in the field of space physics at the University of Rostov-on-Don. *Pravda* newspaper frontpaged two columns on this Doctor's thesis. In 1965 he was elected Senior Research Fellow, II grade, and in 1973 became Professor.

With the establishment of the National Committee for Space Research in January 1967 he was elected its Secretary. Since 1973 he has been Vice-President and since 1977 President of this Committee.

From 1972 to 1975 held the post of Deputy Director of the Centre for Earth Sciences. Between 1973 and 1977 he was Scientific Secretary of the Bulgarian Academy of Sciences. Since 1977 he has been member of the Presidium of the Bulgarian Academy of Sciences. Since the establishment of the Group for Space Physics (in 1969) K. B. Serafimov has been its Deputy Director and in 1973 became Director of the Group. In 1974 this Group was transformed into the Central Laboratory for Space Research. He has been its foundator and Director ever since. From 1979 to 1982 he was Director of the Astronomical Department with the National Astronomical Observatory.

In 1969 K. B. Serafimov became Vice-President and since 1978 he has been President of the Bulgarian Astronautical Society. Since 1977 he has been member of the Presidium of the Union of Bulgarian Scientists, and since 1982 — Secretary General of this Union.

He has been President of the National Committee for Radio Sciences since its establishment in 1975. He is member of the National Committee for Geodesy and Geophysics and of other bodies. Since its establishment in 1980 he has been President of the Council for Technical and Scientific Research

of the Youth. He is Vice-President of the Council of Science Promotion at the Bulgarian Academy of Sciences.

Kiril Serafimov is Editor-in-Chief of the *Space Research in Bulgaria* journal, member of the Bureau of the Editorial Board of the *Review of the*

Bulgarian Academy of Sciences, and on the Editorial Board of the international scientific journal *Advances in Earth-Orientated Applications on Space Technology*, as well as of the *Bulgarian Geophysical Journal, Military Technology, Fatherland, Science and Technology for Youth, Youth, Wings*, etc. He was scientific observer for the *Zemedelsko Zname* newspaper between 1968 and 1979. Since 1979 he has been scientific observer for the *Rabotnichesko Delo* newspaper.

He is the author of more than 420 scientific contributions (developments, publications, inventions) and of five monographs. His works were published in international issues of repute. Over 600 of his citations have been referred to in Bulgaria and abroad. A series of his studies have been adopted as UN documents and by other international organizations.

The principal scientific achievements of Academician Prof. Dr Kiril Serafimov lie within three domains: ionospheric, magnetospheric, and radiowave propagation physics, space instrumentation and satellite communications. The establishment and successful development of the vertical ionospheric probing, of the space plasma direct measurements with satellites and rockets, the design and construction of Bulgarian space instruments, the measurement of natural optical emissions and the theory of space communications have been led by him. Series of background works on space problems in the field of social sciences are also his contribution. He supervised and actively participated in determining the optimal location of the Bulgarian station for space communications and of the Bulgarian telemetric station, an effort highly acknowledged by the Soviet specialists. He was the principal investigator in the elaboration of many themes on the electromagnetic compatibility of various radio-electronic techniques, radio goniometry, etc. K. B. Serafimov was the programme manager of the Bulgarian participation in the experiments with the Soviet satellites COSMOS-261, 348, 381 and the international spacecraft INTERCOSMOS-2, 8, 12, 14, 19, as well as with the heavy geophysical rockets VERTICAL-3, 4, 6, 7, 10, etc. He is the initiator and the head of the Bulgaro-Indian project for studying the precipitating proton particles over the equator. Theoretical and ground-based studies have been made within this project and two Indian CENTAUR-II rockets with Bulgarian and Indian equipment were launched. He was President of the Programme Committee for the flight of the Bulgarian cosmonaut and was the initiator and head of some experiments for this flight within the field of space physics and remote sensing of the Earth. He supervised the elaboration of all Bulgarian systems, instruments and devices for the SALYUT-6 orbiting station. He was the initiator and the principal investigator of BULGARIA-1300 space project. METEOR-PRIRODA and INTERCOSMOS-BULGARIA-1300 satellites were launched within the framework of this project in 1981 with complex Bulgarian equipment.

The contribution of Academician Kiril Serafimov to the economic problems of the space research, to the orientation and organization of the large space scientific-production groups and to the optimization of space operations are of significant importance for the increase of efficiency in space study and exploration. The first studies into the history of space research in Bulgaria were made by him and he made the first original chronology of the INTERCOSMOS history. Together with the Bulgarian cosmonaut Georgi Ivanov he worked on two interesting problems: the effect of the space era on the cultural development, and the effect of space flights on global human psychology. In his fundamental monograph on socialist integration in space he outlined the main trends of study within this extremely effective and efficient domain of cooperated efforts of the socialist countries.

Academician Serafimov founded and supervised the developments of the space technology transfer in Bulgaria. He initiated and is heading a significant part of the multiplication use of space technologies, methods, means, circuitry solutions, constructions and other elaborations in the non-space fields of the national economy.

He is President of the Specialized National Scientific Council of Geophysical Sciences at the Higher Testimonial Committee and of the Scientific Councils at the Central Laboratory for Space Research and the Astronomical Department with the National Astronomical Observatory at the Bulgarian Academy of Sciences. He was elected Corresponding Member of the Bulgarian Academy of Science in 1977 and Regular Member in 1984.

Academician Serafimov has been Corresponding Member of the International Astronautical Academy in Paris since 1969 and Regular Member since 1984. He has been member of the Programme Committees for the International Astronautical Congresses since 1972. He has held membership in the Bureau of the World Committee for Space Research (COSPAR) since 1975. He was the Chairman of the Working Group G. 7 of the International Radio Scientific Union (URSI). Kiril Serafimov has presided over Section I "Upper Atmosphere and Magnetosphere of the Earth and the Planets" of INTERCOSMOS since its establishment. He was President of the Permanent Working Group on Space Physics (1974-1975; 1981-1982), and President of the entire INTERCOSMOS programme (1979-1980). From 1974 to 1982 he presided over the Bulgarian side of the Bulgaro-Indian Commission for Scientific and Technical Cooperation and since 1976 has been President of the Bulgarian side of the Commission for Scientific and Technical Cooperation with Greece. He was awarded medals by the Intercosmos Council, the Academies of the GDR, Poland and other countries.

He led the Bulgarian delegations on the Scientific and Technical Subcommittee of the UN for the Peaceful Exploration of Outer Space. At the second conference of the UN on this subject (UNISPACE-82) he was nominated Vice-President of the Conference. He was awarded the Order of Cyril and Methodius, Ist grade (1969), the Gold Order of Labour (1973), Marin Drinov Medal, the Gold Decoration of the Bulgarian Astronautical Society, the Order of Georgi Dimitrov (1984) and received many other government decorations and distinctions from other organizations. Since 1980 he has been a Honoured Scientist of Bulgaria.

The activity of Academiciam Kiril Serafimov within the entire framework of the Bulgarian Academy of Sciences is extremely useful. He manifested capacities of a learned, capable contemporary scientist with broad views and initiative, as well as talent for organization. In a short period the Central Laboratory for Space Research at the Bulgarian Academy of Sciences under the leadership and with the stimulating help and assistance of the Presidium and the President of the Academy, Academician A. Balevski, has developed into a centre for research and exploration of space.

When a new space project or elaborations come into being, Academician K. Serafimov would set up the problem in such a way that the respective specialists, scientists, constructors or technicians would willingly respond personally, through their work, results, plans, suggestions. This ability of his is enthusiastically supported by the young staff of the Central Laboratory for Space Research, who as a rule look forward to facing unresolved and important problems in the field of space research.

Special mention deserves the capacity of Academician Serafimov to work with the young specialists. He has repeatedly stated that "... the young people should be given the opportunity to develop not on the basis of qualification alone, but on their actual creative achievements...".

Highly valued is Academician Serafimov's activity within the framework of the INTERCOSMOS programme as one of its founders, maintaining allround, long-term and extremely successful cooperation with the USSR, the Soviet science, scientists and specialists. Multiple are the joint scientific projects in space testifying to the great creative talent of the hero of the jubilee.

He is a brilliant and worthy representative of Bulgarian science and technology, his opinion and recommendations are sought and highly esteemed at the UN forums, COSPAR congresses, the administration of INTERCOSMOS, the programme and nomination committees of IAA, IAF, etc.

Academician K. Serafimov has published many works in this country and abroad. His overall activity for the establishment and implementation of projects and studies, for the results obtained is valued extremely high. He was flatteringly described in the recently published book by the first Bulgarian cosmonaut Col. Eng. G. Ivanov *Flights*. On page 179 it reads "... I've only heard about Serafimov. But I understood that he is a man of inspiring personality, combining the 'projective' and 'generating' features of a scientist and organizer, exclusively dilligent and capable of extreme physical efforts and hypertense mental activity. Author of many scientific works of worldwide importance, promoter of science, he is a skillful, temperamental and well-founded publicist. So, no wonder, that he successfully represents our country on the international space field and the world space forums, that he is member of many national and international organizations. The energy and ambition he invested in our training were only part of his entire contribution to us, along with purely scientific cooperation. We were lit up by his noble flame and e xperienced his passion and ambition to rank our Fatherland among the leading space countries...."

At his 50th birthday and the 25th anniversary of his scientific activity let us wish him good health, greater and still more significant success in the study and exploration of space for the well-being of our dear Socialist Republic of Bulgaria.

Corr. Member, Prof. D Mishev; Sen. Res. Dr F. I. Kutiev;
Prof. Dr M. M. Gogoshev; Sen. Res. Dr F. S. Chapkunov

BULGARIAN ACADEMY OF SCIENCES

SPACE RESEARCH IN BULGARIA, 5

Sofia · 1986

Analytic Approximation of Integral Intensity of the Line λ 630 nm

K. B. Serafimov

The deduction of the quantity relationships between the airglow and the upper atmospheric parameters provide for the complete analysis of the phenomena in this medium. The aim of this paper is to obtain the approximate analytic expressions for the integral intensity I of the red oxygen line λ 630 nm, generated in the upper atmosphere of the earth. The formulae for the volume emission rate dI/dh, obtained in [1, 2], shape the background for these expressions based on the models for dI/dh in [3]. The latter are based on the model for the neutral atmosphere CIRA-72 and the International Reference Ionosphere IRI-75. The analysis of the new models for dI/dh in agreement with CIRA-79 and IRI-79, as well as the models based on MSIS, combined with IRI (see [4]), do not change the nature of the analytic expressions. Only their digital characteristics are changed. Through the expressions thus deduced for the integral intensity I, in dependence on the parameters of the models for the neutral upper atmosphere and for the ionosphere, a possibility is provided to resolve series of direct and reverse problems — from the known parameters to determine the intensity, or from the known intensity, combined with measurements on the intensity of the line λ 135,6 nm and single measurement on the local electron density, to measure the values of the maximal electron density N_mF (or its respective critical frequency f_0F); of the height of this density h_mF and the constant A_0 of the distribution $N(h)$ in agreement with IRI — see the method in [5]. On the other hand, such expressions enable us to consider the effects of various factors determining the intensity of the line λ 630 nm, and to compare the models of the neutral atmosphere and the ionosphere.

Complete Expressions for the Intensity I_{630}

In [1] from the general expression for the volume emission rate

$$\frac{dI}{dH} = \frac{KA_{630}}{A} \frac{\gamma_1 [O_2] N dh}{[1 + d(h)/A][1 + B(\bar{h})]} \tag{1}$$

approximation of the denominator is obtained

$$[1 + d(h)/A][1 + B(h)] \approx \zeta_0(h_0F) e^{-\rho_1(h - h_0F)} = \zeta(h), \tag{2}$$

where $K=1$, $A_{630}=0{,}069\ s^{-1}$, $A=0{,}0091\ s^{-1}$, N — electron density, $d(h)$ denotes the total deactivation of collisions of excited oxygen atoms in state $O(^1D)$ with neutral nitrogen molecules and with the electrons: $B(h)\gamma_1[0_2]/\alpha_1 N + \gamma_2[N_2]/\alpha_2 N$, where γ_1 and γ_2 are respectively the coefficients of the exchange reactions between the ions of the atomic oxygen and the neutral oxygen, or the nitrogen molecules; and α_1 and α_2 are the coefficients of the dissociative recombination for ions O_2^+ and NO^+, respectively. For the values of the examined coefficients and their temperature, temporal and spatial variations see [1, 2]. In agreement with [1] at midgeographic latitudes ($\varphi=45°$) in 00^h summertime under $R=10$ ($T_{ex}\approx 550°K$) and $h_0F\approx 180$ km, we have $\zeta_0(180)\approx 347{,}4$ and $p_1\approx 0{,}4$.

In agreement with IRI-79 for $N(h)$ under $h\geq h_mF$ (further for simplification we shall use $N_mF=N_m$ and $h_mF=h_m$) we have

$$N(h)=N_m\left[A_1/\left(1+\frac{h-h_m}{A_0}\right)^{A_2}-A_3\exp\left(-A_4\frac{h-h_m}{A_0}\right)\right], \tag{3}$$

where: A_1 — constant of two fixed values (for low and high solar activity, see IRI); $A_2=2$ (at low solar activity); $A_3=3$ (at high solar activity); $A_3=A_1-1$; $A_4=A_1A_2/(A_1-A_2)-0{,}05$. It is clear that under known solar activity all the constants are known from IRI, excluding A_0, which is either taken from IRI or specified through measurements similar to those in [5]. Expressions for $N(h)$ are given in IRI for $h\leq h_mF$ which introduce series of new constants. But we use in [5] the known fact that the circummaximum area of the F-region has distribution very close to the parabolic one and is characterized with symmetry with reference to h_mF. Therefore, we use expression (3) for $h\leq h_mF$ also up to heights of about 180-240 km, and in this region in agreement with [2, 3, 4] the airglow with λ 630 nm is initiated. For the purpose we only substitute $h-h_m$ with the argument h_m-h.

We have shown in [1, 2] that $\zeta(h)$ is given with the expression (2) up to a height of about 280 km over the earth. At $h\geq 280$ km, we have $\zeta\approx 1$. Therefore, we analyse the following cases:

1. Region with $\zeta=1$ ($h\leq 280$ km).

This case can be divided into the following subcases, considering the location of h_mF:

1.1. $h_mF<280$ km.

The airglow occurs in three parts: a) $h_m\leq h<280$ km; b) $h\leq h_m$; c) $h\geq 280$ km. We denote with r, g and n the respective parts of the intensity

$$I=I_r+I_g+I_n. \tag{4}$$

a) $h_m\leq 280$ km

For low solar activity, the following expression for I is obtained from (1), (2), (3)

$$I_r=I_{r_1}+I_{r_2}; \tag{5}$$

$$I_{r_1}=\frac{KA_{630}}{A\zeta_0}\gamma_1 0_2 J_0(180)N_mA_1\int_{h_m}^{280}\frac{e^{-(p_2-p_1)(h-180)}}{\left(1+\frac{h-h_m}{A_0}\right)^2}dh. \tag{6}$$

The exponential approximation for the altitudinal distribution of the molecular oxygen $[0_2](h)\approx[0_2]_0(180)e^{-p_2(h-180)}$ versus the possibly lowest boundary of the airglow of 180 km is considered in the yielding of (6). It is considered that, regardless to the complex nature of the temperature (and therefore altitudinal) variations of γ_1, in agreement with (1) we may consider that

$\gamma_1 \approx 1{,}60\ 10^{-11}\ \text{cm}^3\ S^{-1}$ in the examined altitudinal region. It follows from (6) that

$$I_{r_1} \doteq K_1 N_m A_0 e^{-(p_2-p_1)(h_m-A_0-180)} \left\{ \frac{-e^{A_0(p_2-p_1)U}}{U} - A_0(p_2-p_1)E_i[A_0(p_1-p_2)U] \right\}_{U=1} \frac{280-A_0-hm}{A_0}, \tag{7}$$

where $K_1 = \frac{KA_{630}}{A\zeta_0} \gamma_1 [0_2]_0 (180) A_1$; E_i is the generally accepted denomination of the exponential-integral function.

At high solar activity ($R \geq 100$) we have

$$I_{r_1} = K_1 N_m \int_{h_m}^{280} \frac{e^{-(p_2-p_1)(h-180)}}{\left(1+\frac{h-h_m}{A_0}\right)^3} dh; \tag{8}$$

$$I_{r_1} = K_1 N_m A_0 e^{-(p_2-p_1)(h_m-A_0-180)} \left\{ \frac{-e^{-(p_2-p_1)A_0U}}{2U^2} + \frac{(p_2-p_1)A_0 e^{-(p_2-p_1)A_0U}}{2U} + \frac{(p_2-p_1)^2 A_0^2}{2} E_i[A_0(p_1-p_2)U] \right\}_{U=1}^{\frac{280-h_m-A_0}{A}}. \tag{9}$$

The expression for I_{r_2} does not depend on the solar activity and we obtain

$$I_{r_2} = \frac{KA_{630}}{A\zeta_0} \gamma_1 [0_2]_0 (180) A_3 N_m \int_{h_m}^{280} e^{-(p_2-p_1)(h-180)} e^{-A_4 \frac{h-h_m}{A_0}} dh; \tag{10}$$

$$I_{r_2} = \frac{K_2 A_0 N_m e^{-(p_2-p_1)(h_m-180)}}{(p_2-p_1)A_0 + A_4} \left\{ 1 - e^{-[(p_2-p_1)A_0+A_4]\frac{280-h_m}{A_0}} \right\}, \tag{11}$$

where

$$K_2 = \frac{KA_{630}}{A\zeta_0} \gamma_1 [0_2]_0 (180) A_3. \tag{12}$$

b) $h \leq h_m$

As we have already shown, in this case we substitute in (3) the expression $h-h_m$ with h_m-h, which is yielded at low solar activity

$$I_{g_1} = K_1 N_m A_0 e^{-(p_2-p_1)(h_m+A_0-180)} \left\{ -e^{A_0(p_2-p_1)U} + A_0(p_2-p_1)E_i[A_0(p_2-p_1)U] \right\}_{U=1}^{\frac{h_m+A_0-180}{A_0}}; \tag{13}$$

$$I_{g_1} = \frac{K_2 A_0 N_m e^{-(p_2-p_1)(h_m-180)}}{A_4 - (p_2-p_1)A_0} \left\{ 1 - e^{-[A_4-(p_2-p_1)]\frac{h_m-180}{A_0}} \right\}. \tag{14}$$

At high solar activity we have

$$I_{g_1} = K_1 N_m A_0 e^{-(p_2-p_1)(h_m+A_0-180)} \left\{ -\frac{e^{(p_2-p_1)A_0U}}{2U^2} - \frac{A_0(p_2-p_1)e^{(p_2-p_1)A_0U}}{2U} + \frac{(p_2-p_1)^2 A_0^2}{2} E_i[A_0(p_2-p_1)U] \right\}_{U=1}^{\frac{h_m+A_0-180}{A_0}}. \tag{15}$$

I_{g_2} has the form of (14).

c) $h>280$ km

This case is treated under $\zeta=1$.

1.2. $h_mF>280$ km

In this case the total intensity is also formed in three layers: a) $180\leq h\leq 280$ km$/\zeta+1$; submaximum region; b) $280\leq h\leq h_m/\zeta=1$; submaximum region, and c) $h>h_m/\zeta=1$; abovemaximum region. Cases b) and c) will be considered for $\zeta=1$. For case a) we use (13) and (14) for low and high activity respectively and substitute the bottom boundary in both cases with $(h_m+A_0-280)/A_0$.

2. $\zeta=1$ ($h>280$ km)

2.1. $h_mF<280$ km

We have again the subcases and the respective componets given by the indices r, g and n, shown in 1.1. We use for the components r and g the already deduced expressions (7) and (9), (11), (13), (14), (15). The following dependence is given for the component n

$$I_n=I_{n_1}+I_{n_2}, \tag{16}$$

where at low solar activity

$$I_{n_1}=\frac{KA_{630}}{A}\gamma_1[O_2]_0(180)N_mA_1\int_{280}^{h_r}\frac{e^{-p_2(h-180)}}{\left(1+\frac{h-h_m}{A_0}\right)^2}dh; \tag{17}$$

$$I_{n_1}=K_3N_mA_0e^{-p_2(h_m-A_0-180)}\left\{\frac{-e^{-p_2A_0U}}{U}-p_2A_0E_i(-p_2A_0U)\right\}_{U=\frac{280+A_0-h_m}{A_0}}^{\frac{400+A_0-h_m}{A_0}}. \tag{18}$$

At high solar activity

$$I_{n_1}=K_3N_mA_0e^{-p_2(h_m-A_0-180)}\left[\frac{e^{-p_2A_0U}}{2U^2}+\frac{p_2A_0e^{-p_2A_0U}}{2U}+\frac{p_2^2A_0^2}{2}E_i(-p_2A_0U)\right]_{U=\frac{280+A_0-h_m}{A_0}}^{\frac{600+A_0-h_m}{A_0}}, \tag{19}$$

where $K_3=KA_{630}\gamma_1[O_2]_0(180)A_1/A$.

It is considered in (18) and (19) that in agreement with [1, 3, 4] the upper boundary of the airglow with λ 630 nm is about $h_r\approx 400$ km at low activity and about 600 km at high activity. For I_{n_2} we have

$$I_{n_2}=\frac{K_4A_0N_me^{-p_2(h_m-180)}}{p_2A_0+A_4}\left[e^{-(p_2A_0+A_4)\frac{280-h_m}{A_0}}e^{-(p_2A_0+A_4)\frac{h_r-h_m}{A_0}}\right], \tag{20}$$

where $K_4=KA_{630}\gamma_1[O_2]_0(180)A_2/A$.

2.2. $h_mF>280$ km

In this case also three components of the indices r, g and n are available, and I_{r_1} is determined with (13) or (15) for low and high activity, respectively, but with substituted bottom boundary: instead of $U=1$, $U=\frac{h_m+A_0-280}{A_0}$ is used; expression (7) is justified for the component I_{g_1} with substituted argument — instead of $h-h_m$, h_m-h. Expressions similar to (18) of upper boundary equal to an unit are obtained. Dependences such as (18), (19) and (20)

are used for the components I_n with substituted bottom boundary, namely $U=1$.

With the dependences here deduced, various ionospheric or aeronomic parameters can be determined and the respective equations are solved in graph-analytical manner similar to the method in [6] or the *regula falsi* method. The data from IRI can be used in the latter case as orientation for the search of the respective solutions.

Discussion and conclusions

According to IRI, the cases with $h_mF \leq 280$ km are quite rare. In fact, our observations on midgeographic latitudes contradict this concept since often $220 \leq h_mF \leq 280$ km, see summaries in [2, 10].

For the computing procedures it should be considered that in many cases (for example at high values of the power index in the decreasing exponential functions or at large arguments of the integral-exponential function) significant simplifications of the expressions deduced here are obtained. In agreement with the method developed in [5, 7] the expressions of the intensity of the red oxygen line, together with those of the intensity of the ultraviolet line with λ 135,6 nm and a local measurement of the electron density provide yield of parameters N_m, A_0 and h_m. This is the determination of all the parameters necessary for the computation of the maximal usable frequencies (MUF) in radiocommunications. On the other hand, the determination of the profile $N(h)$ of the electron density in this manner and its correlation with the concrete measurements of the mentioned airglow emissions and with a value of the electron density, enable the performance of improvement and updating of the IRI model. Therefore, its adequacy is enhanced.

The expressions obtained contain the unknowns N_m, h_m and A_0 of very complex relationships. But their graph-analytic solution or through the *regula falsi* method is not difficult in the application of the orientating values of the IRI, or from the ionospheric models of the CCIR.

Both through the dependences obtained here and through the formulae found for the intensity of the emission with λ 135,6 nm in [5, 8, 9] the background for the complete consideration of all the factors for the generation of the most important oxygen lines in the airglow and for the serious mathematical theory of this phenomenon in the upper atmospheres of the planets and the earth is compiled.

References

1. Serafimov, K. B. — Bulg. Geophys. J., 3, 1977, 3, 34.
2. Serafimov, K. B. Space Res. in Bulgaria, Sofia, 1979 (Russ.).
3. Serafimov, K. B., M. Gogoshev, Ts. Gogosheva. — Geomagnetism and Aeronomy, 17, 1977, 6, 1044.
4. Gogosheva, Ts., K. Serafimov. Optical Testing of IRI and MSIS Model, Intercomparison. — COSPAR, 23th Plen. Mtg. Budapest, Rep. C. 3. 3. 8, 1980.
5. Serafimov, K. B. — Space Res., 20, 1982, 5, 736 (Russ.).
6. Tinsley, B. A., J. A. Bittencourt. — J. Geophys. Res., 80, 1980, 2333.
7. Serafimov, K. B. — Compt. rend., 32, 1981, 11, 36.
8. Serafimov, K. B. — Bulg. Geophys. J., 6, 1980, 6, 25.
9. Serafimov, K. B. — Compt. rend. Acad. Bulg. Sci., 33, 1980, 2, 199.
10. Serafimov, K. B. Physics of the Middle Ionosphere, Sofia, 1970 (Russ.).

Аналитическая аппроксимация интегральной интенсивности линии λ 630 nm

К. Б. Серафимов

(Р е з ю м е)

На основе модели нейтральной атмосферы CIRA-79 и Интернациональной референтной ионосферы IRI-79 выведены полные аналитические выражения интенсивности красной линии кислорода на длине волны λ 630 nm. Рассмотрены различные случаи и представлены полные формулы для I_{630} в зависимости от взаимного расположения высоты максимальной электронной концентрации N_mF и высоты 280 км (до которой необходимо учитывать фактор в знаменателе интегральной интенсивности). Полученные таким образом выражения дают возможность точного решения ряда прямых и обратных задач аэрономии, в том числе определения ионосферных параметров N_mF, h_mF и A_0 (IRI-модели) посредством оптических и плазменных измерений.

BULGARIAN ACADEMY OF SCIENCES

SPACE RESEARCH IN BULGARIA, 5

Sofia . 1986

The Outer Ionosphere at Mid- and Low Latitudes

I. S. Kutiev

Introduction

Satellite data came first within our reach in 1969, with the beginning of joint investigations with the working team of Galperin from the Space Research Institute in Moscow on the joint usage of ground-based data and of data obtained from the COSMOS-261 and COSMOS-348 satellites. In 1969 broad-scale research work was started in cooperation with the working team of Prof. Gringaus from the Space Research Institute in Moscow, in the field of the processing and geophysical interpretation of the measurements of ion density, made by INTERCOSMOS-2 satellite. These were the first for Bulgaria methodological investigations on the processing and interpretation of the volt-ampere characteristics of the spheric ion traps. That resulted in the establishment of reliable methods for the separation of oxygen and carbon ions which have found a broad application in further experiments. The first Bulgarian instrument, jointly developed by our Institute and the working team of Gringaus, was a combination of spheric ion traps and the Langmuir cylindrical probe, applied aboard INTERCOSMOS-8 in 1972. On the grounds of the data obtained from these two satellites in the Central Laboratory for Space Research there were conducted a number of studies on the structure of the equatorial outer ionosphere, on the longitude peculiarities in the distribution of ion density under the conditions of a geomagnetic field, on the structure and time variations of the midlatitude trough, etc. Probe instruments for sounding the ionospheric plasma flew later on aboard the INTERCOSMOS-12, 14 and 18 as ingredient of scientific payload with different purposes. With the help of INTERCOSMOS-12 there was studied the behaviour of the midlatitude trough at an altitude of 700 km, with special attention being paid to the behaviour of the O^+ and H^+ ions. The INTERCOSMOS-14 was aimed at studying the waves occuring in the outer ionosphere where passive measurements were made only of the variations of the ion density by means of a spherical ion trap. Spherical ion traps and a Langmuir cylindrical probe flew aboard the INTERCOSMOS-19, equipped also with an ionospherical sounder besides the other instruments for scientific researches.

Aboard INTERCOSMOS-BULGARIA-1300 satellite, launched on August 7th 1981, there was a payload of 11 instruments, aimed at researching the interactions of ionosphere and magnetosphere. The values measured involve the pa-

rameters of thermal plasma and its drift velocity, the AC and DC electric fields, the magnetic fields of the earth, the energy spectrum of protons and electrons, and the intensity of the atmospheric emissions in the visible and in ultra-violet portion of the spectrum. Recently, on the grounds of these data there has begun the study of the structure of the equatorial ionosphere and of the polar oval, the behaviour of the SAR-arcs, the double electrostatic layers, the particle acceleration, etc.

Bulgarian participation is significant in experimenting rockets of the VERTICAL type, launched from a midlatitude station and reaching an altitude of up to 1500 km. Using the vertical profiles of outer ionosphere provided by the rockets of the VERTICAL-3, 4, 6 and 10, obtained within almost one decade, there were conducted studies on the ion composition, on the structure and dynamics of the ionospherical plasma.

This paper attaches special attention to some investigations, conducted by researchers from the Central Laboratory for Space Research in Sofia. Among the multitude of their findings this paper presents only those which give a complete idea of the physical conditions in outer ionosphere at low and midlatitudes, independently of the fact that these results have been obtained over a period of more than thirteen years.

Latitude Variations of Ion Density

The latitude variations of ion density have been extensively studied, using data from spherical ion traps (SIT) on board INTERCOSMOS-2 and 8, and those from the retarding potential analyzer (RPA) on OGO-6 satellite*.

The latitude distribution of O^+ ion density measured by INTERCOSMOS-8 between 280 and 580 km height in the afternoon and evening hours has been analyzed in [1, 2]. Fig. 1 gives profiles of the O^+ density between 50° and — 50° diplatitude for several consecutive longitudes. The local times of the measurements lie between 15.30 and 19.30 h. In the front panel an average satellite altitude shows the dependence of ion density on height. The orbits have been chosen with a view to the satellite passing the equatorial region around the maximum of F-layer where the anomaly is better pronounced. The main feature is a double maximum distribution of ion density. The two crests are situated at about 15° on both sides of the geometrical equator. At longitudes between —50° ano 7° ion density reaches its minimum at about 10° north of the equator. These longitude peculiarities will be analyzed further on. Daytime distribution of ion density around the maximum of the F-layer, shown in Fig. 1, is in full conformity with the results of the previous investigations, for example [3, 4]. Meridional profiles of ion density in the evening hours (17.00-22.30 LT) are shown in Fig. 2. It displays clearly the distortion of the daytime anomaly. The equatorial depletion is now shifted to the north to a latitude of about 15-20°, while the southern crest acquires higher density. A tendency can be observed for the latter crest to shift towards the equator and for the northern crest to disappear. This picture corresponds to a transition stage towards establishing a steady one-maximum distribution during the night [5, 6]. The local minima, appearing in longitude range (—50°, 60°), are caused by local dynamics of the F-layer, which will be discussed further in this paper.

Model calculations made in [7, 8] show that the daytime F-layer equatorial anomaly has an upper altitude limit. At altitudes above 700 km the crests

* Courtesy of WDC-A for R&S

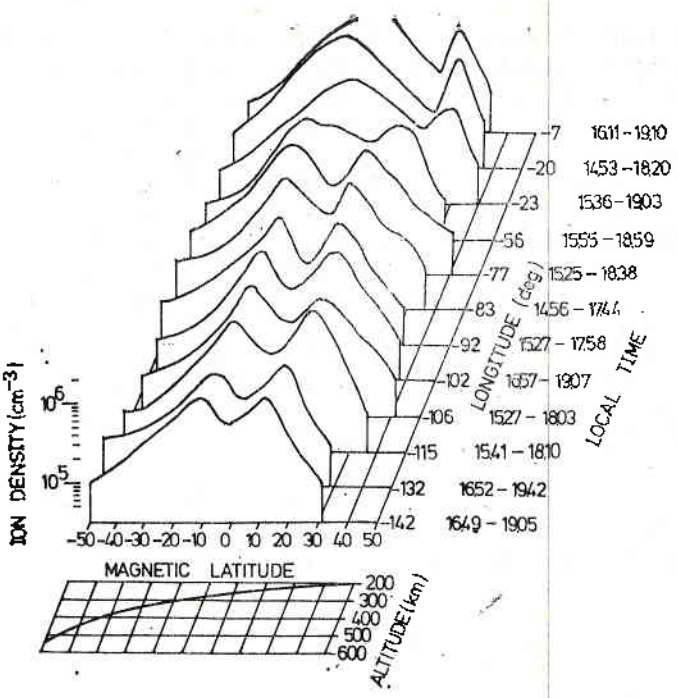

Fig. 1. Daytime 0+ density vs. magnetic latitude

The average altitude of the measurements is drawn in the front panel. Longitudes and local time for every individual profile are given on the right side. The density scale is given on the left side

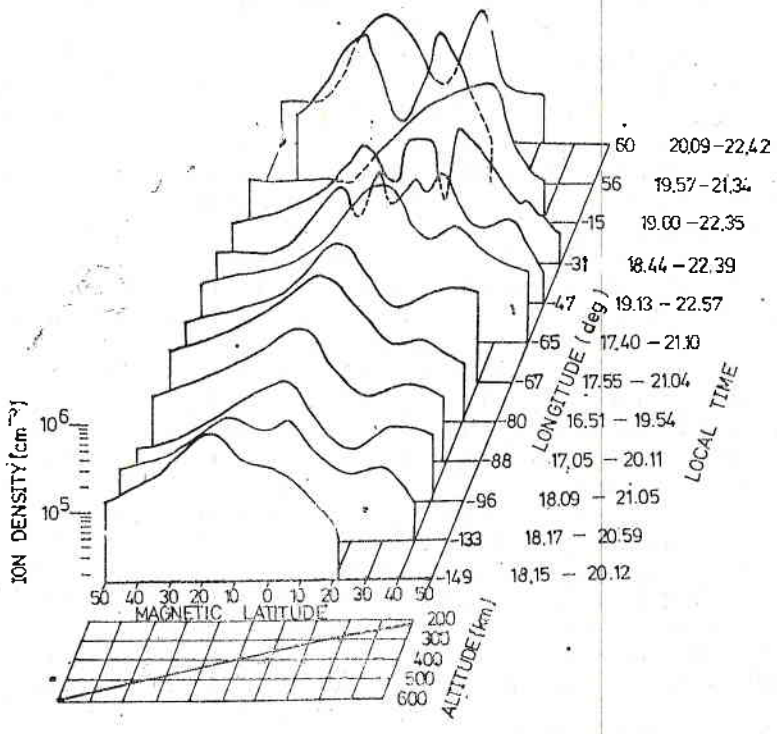

Fig. 2. The same as in Fig. 1. for evening and nighttime conditions

seem to shift towards each other and at altitudes high enough one-maximum distribution of O^+ ion density is established at the equator. Due to an upwad E×B drift in equatorial plane the F-layer goes up to 500-700 km. Being lifted

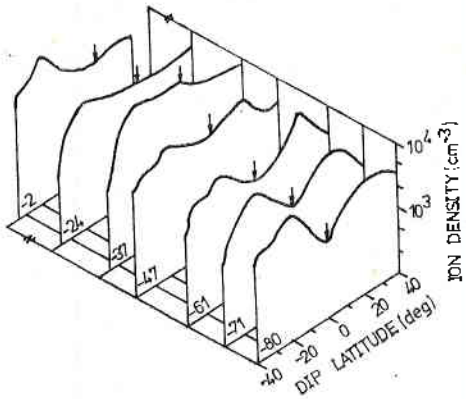

Fig. 3. Nighttime H+density over the equator and midlatitudes taken by the INTERCOSMOS-2, January 3-10, 1970

The density scale is shown on the right side. The average satellite altitude is given in the front

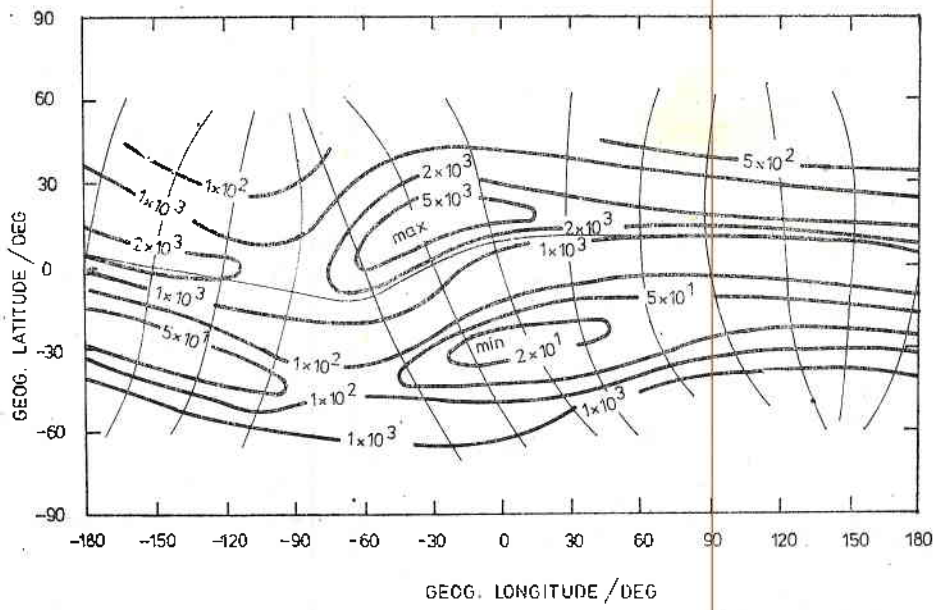

Fig. 4. Contours of constant nighttime O+ density values for altitudes about 1000 km (the heavy lines)

The data are taken by OGO-6 in the summer of 1969 and 1970. The thin lines represent the magnetic equator and magnetic meridians

higher than the normal midlatitude F-layer, the equatorial F-layer provides the crest regions with ionization which diffuses down along magnetic field lines. Applying this 'fountain effect' to helium and hydrogen ions, the author

in [8] has obtained their latitude distribution. According to this model the helium and hydrogen ion layers which lie above that of the O^+ ions, are lifted by E×B drift to greater heights and subsequently they fill magnetic tubes at higher invariant latitudes. An ion distribution measured by a satellite flying at about 1000 km can be represented as follows:

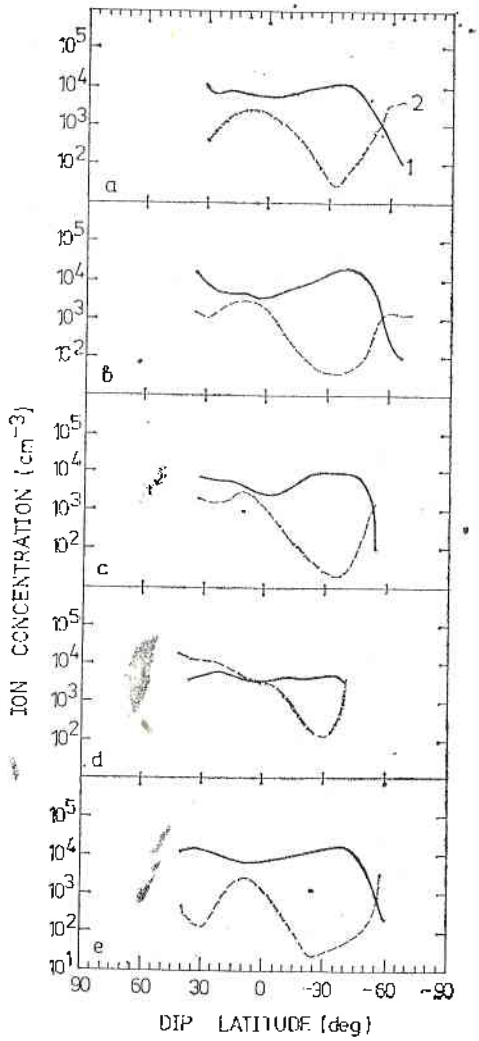

Fig. 5. Nighttime O^+ and H^+ density for five individual passes of OGO-6 in different longitude zones

Apogee of 1090 km is at the dipequator, with the altitude at ±60° diplatitude being about 800 km. 1 — H^+; 2 — O^+; longitude: *a* - · 172°, *b* — 116°, *c* — 72°, *d* - · -40°, *e* — -134°

-· Maximal O^+ density and minimal H^+ density at the equator and minimum O^+ and maximum H^+ densities at midlatitudes;

-- The behaviour of He^+ density should be somewhat in the middle: its maximum density should be found equatorward from H^+ maximal density;

— Minimum He^+ density will appear at the equator, if the He^+ layer is elevated above 1000 km, otherwise a maximum He^+ should be expected there.

Similar behaviour is observed by INTERCOSMOS-2 satellite [9, 10] and ISIS-2 [11]. Latitude distribution of nighttime H^+ density at about 1000-1100 km altitude is shown in Fig. 3 pertaining to a number of INTERCOSMOS-2 transequatorial passes during the period of January 1-14, 1970 [12, 13]. The apogee is near to the equator at a height of about 1100 km. The latitude profiles shown here reveal a two-maximum distribution, resembling the shape of the daytime F-layer equatorial anomaly. The crests of H^+ density are found between 10° and 30° on both sides of the equator. Approximately half a year ago, also in the maximum solar activity period, data of latitude distribution of O^+ density, at about the same heights were collected by OGO-6 satellite [15]. Contours of oxygen ion density obtained by RPA of OGO-6 [14] during the night at 1000-1100 km are plotted on Fig. 4. If we consider now only the latitude variations we see that the oxygen ions have maximal density slightly northwards from the geometrical equator towards the summer hemisphere. At the opposite side of the equator a deep minimum occurs and at some locations the density appears to be as low as 20 ions per cc. A good idea how the latitude distribution of H^+ and O^+ density should look is given by Fig. 5, where RPA data for several passes of OGO-6 over the equatorial region are presented. The shape

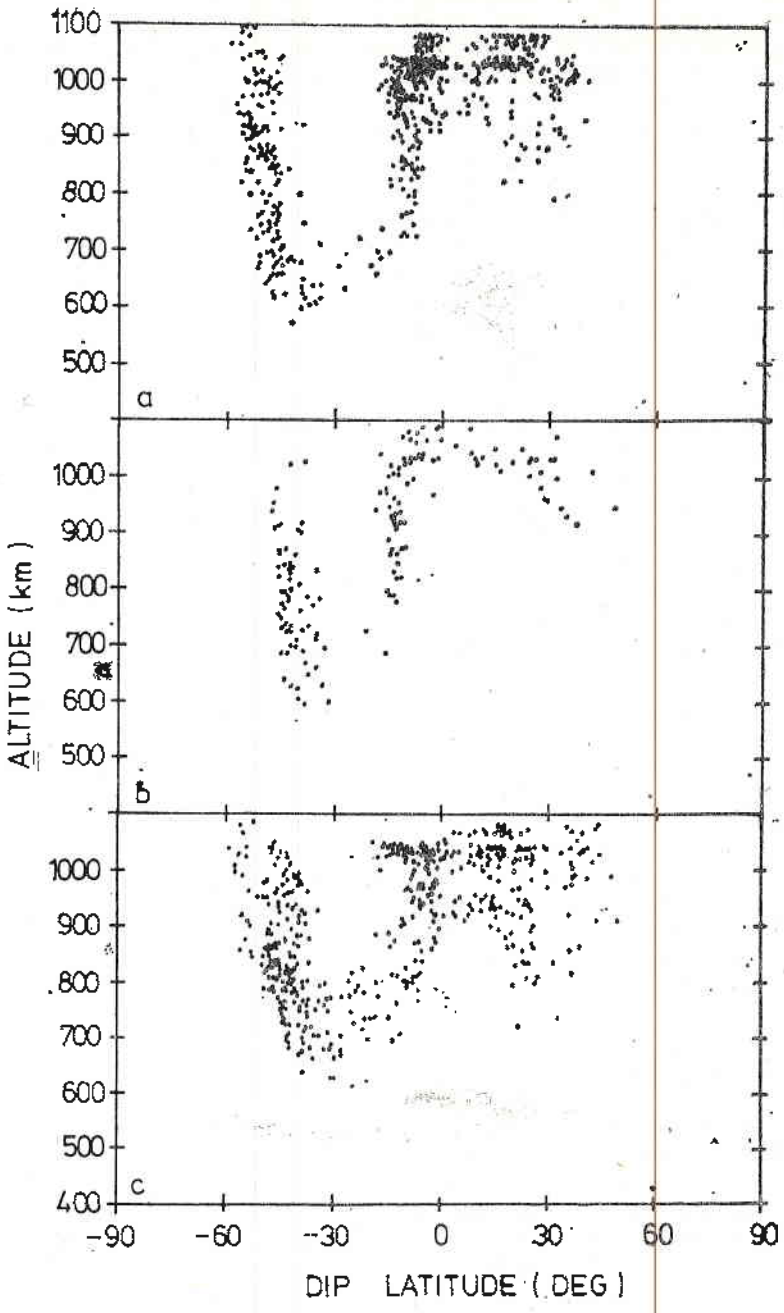

Fig. 6. The altitude dependence of the transition level on the diplatitude in three longitude zones

HMIN=400 and HMAX=1100 indicate the altitude limits over which the data have been taken in summer, nighttime

of H^+ and O^+ densities distribution is in full accord with the 'fountain effect' theory. Winter minimum of oxygen ions at about 30° diplatitude corresponds to a highly exhausted nighttime midlatitude F-region. The relatively shallow summer minimum is a result of the more intensive photoionization during

the day, as well as of the influence of the neutral winds. The action of the latter will be considered further on in the paper. Fig. 5 shows H^+ density almost uniformly distributed over the latitudes considered. Along the orbits where these data have been collected the H^+ and O^+ density reach equal values, several times. The altitude where these densities reach equal values, i. e. the so-called transition level, is a parameter which is used in [15] to visualize some dynamic properties of outer low and midlatitude ionosphere. In Fig. 6 every single point represent a transition level value extracted along the satellite orbit. The transition level (TL) points taken from nighttime data are plotted against their diplatitudes. The three panels of the Fig. 6 show the latitude shape of TL in three longitude intervals: *a* — Eurasian (10°, 150°); *b* — Atlantic (−60°, 10°); and *c* — Pacific (150°, through 180° to −60°). The main feature of these TL profiles is a deep minimum located between 0° and 40° diplatitude, where TL descends to 600 km, while around the equator and poleward end of the latitude region TL is at 1000-1100 km. In [15] it is pointed out that around 18 local time TL is at about 1000-1100 km throughout the region. During the night TL in the equatorial zone remains at the same height, while at midlatitudes a significant decrease of TL occurs. Higher TL values at the poleward edge of the region considered here is due to the abrupt decrease of the H^+ density as it can be seen from the individual passes in Fig. 5. The midlatitude decrease of TL represents the normal nighttime collapse of the F-layer. An interesting feature is the maintenance of the high equatorial TL values during the night. This behaviour is closely associated with O^+ density distribution, shown in Fig. 4. Maximum oxygen ion density occurs at 5°-10° latitude in the summer hemisphere. The existing assymetry in O^+ density along the magnetic field lines over the equator gives support to a diffusion flow from summer to winter side. This O^+ flow keeps a higher O^+ density along the magnetic flux tubes close to the equator, because of which TL heights remain high. The latitude at which the height of TL changes abruptly corresponds to those magnetic tubes which limit from above the transequatorial flow of the oxygen ions. Beyond this latitude the direct support of ionization to winter nighttime F-region is strongly restricted, because of the necessity of conversion of oxygen ions into hydrogen ions and vice versa via a charge exchange reaction.

Longitude Variations

As it has been shown in the preceding section, the latitude profiles of oxygen and hydrogen ions reveal a strong longitude dependence. The overall O^+ density distribution shown in Fig. 4 gives information on large-scale longitude variations of the ion density at a height of 1000 km. The strongest assymmetry along the magnetic meridians occurs between −40° and 20° longitude and the weakest one occurs in neighbouring regions between −100° and −60° longitude. The longitude variations of O^+ density at the heights of the maximum F-layer are shown in Fig. 7 [16]. Here the dots represent measured O^+ density at 30° and −30° diplatitude. The heavy line shows variations of magnetic declination properly adjusted to reveal an excellent correlation with the ion density values. From the *b* section of the figure, representing the summer hemisphere, there can be concluded that the higher ion density along 30° diplatitude is connected with the negative values of the magnetic declination, e. g. the magnetic flux tubes have a westward component. The highest values of the ion density on the summer side of the equator are found at about −30° diplatitude. The same longitude

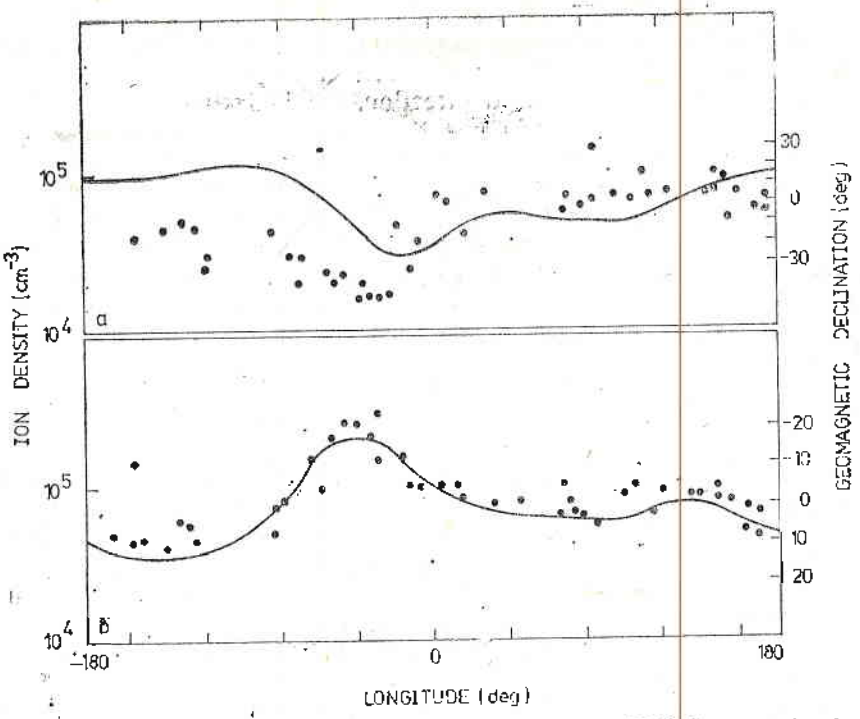

Fig. 7. Nighttime O^+ density vs. longitude taken by OGO-6 at two fixed diplatitudes

The magnetic declination has a scale on the right. This line does not represent an average curve over points, but was adjusted to match the O^+ density variation. *a* – altitude 650-900 km, diplatitude -30°, local time (LT) 22.00-22.30 h; *b* — altitude 450-500 km, diplatitude 30°, LT 22.30-23.00 h

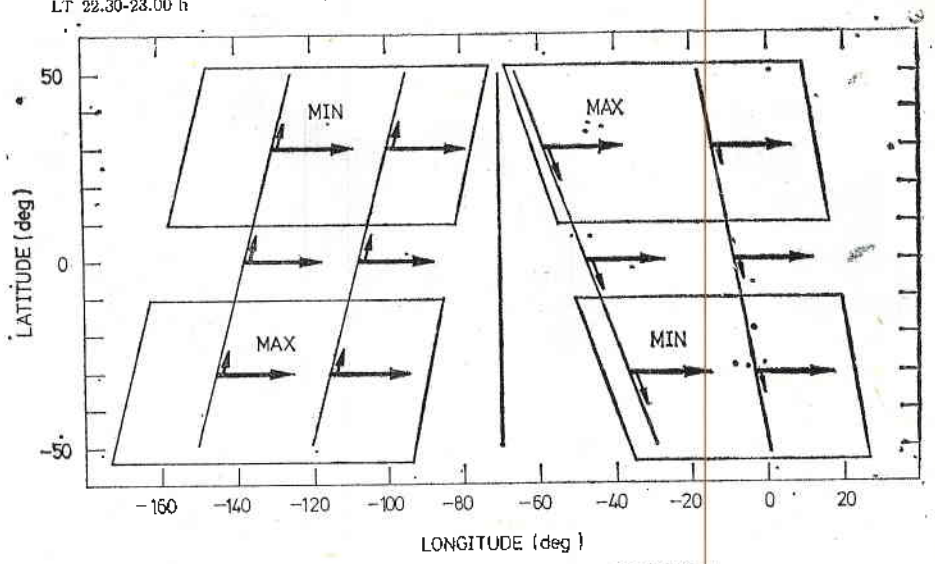

Fig. 8. A sketch representing the neutral wind action on ionization

region from the winter side shows the lowest densities. This behaviour corresponds well to that shown in Fig. 4. A reasonable explanation, given in [17], is demonstrated in Fig. 8. The winds flowing at F-layer heights, preferably

n west-east direction, experience a drag force upon ionization, if the magnetic meridians differ from the north-south direction. Depending on the component of magnetic field lines in the wind direction, the ionization is dragged upward or downward. The light lines in Fig. 8 represent the magnetic field lines in a geographic frame of coordinates. The heavy arrows show the neutral wind direction, and the smaller arrows give the magnitude and the direction of the ion drag along the magnetic field lines. The regions where a satellite could measure enhanced or depleted ionization are also indicated in the figure. The zones marked by MAX correspond to an elevation of the F-layer upwards, and those marked by MIN correspond to a pushing of the F-layer downwards. The sketch in Fig. 7 is in agreement with these in Fig. 4 and 5.

Irregularity Structure

The magnetic field configuration defines not only ionospheric plasma dynamics, but the appearance of irregularity structure as well. With the help of INTERCOSMOS-2 in [18, 19] the character and size of the irregularities in the equatorial F-region in the period of low solar activity have been studied. In Fig. 9 the latitude profiles of the O^+ density between 280 km and 580 km are displayed. In two cases of the profiles the occurence of irregularities is indicated by small bars. This shows that irregularities are found mainly between $-50°$ and $-10°$ longitude and are strongly coupled with sharp depletions in ion density. Similar individual passes of the same satellite are shown in Fig. 10 [20].

The minima in the density depletions are defined by the threshold sensitivity of the ion traps but other measurements, for instance [21], show that such a decrease reaches three orders of magnitude.

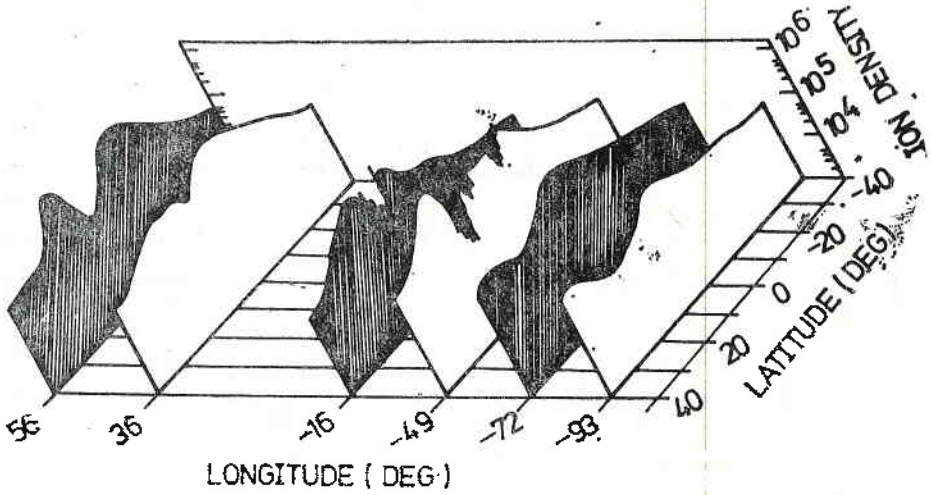

Fig. 9. O^+ density profiles at different longitudes in D months
Vertical bars in the profiles at $-16°$ and $-49°$ longitudes indicate the presence of irregularity structure ; I.T 19.40-22.30 h

Irregularity structure at heights of about 1000 km has been observed by the INTERCOSMOS-2 satellite. In Fig. 11 parts of satellites trajections with irregularities of over 7% of ion current are indicated. The heavy line represents the geomagnetic equator in a geographic frame of coordinates. The space

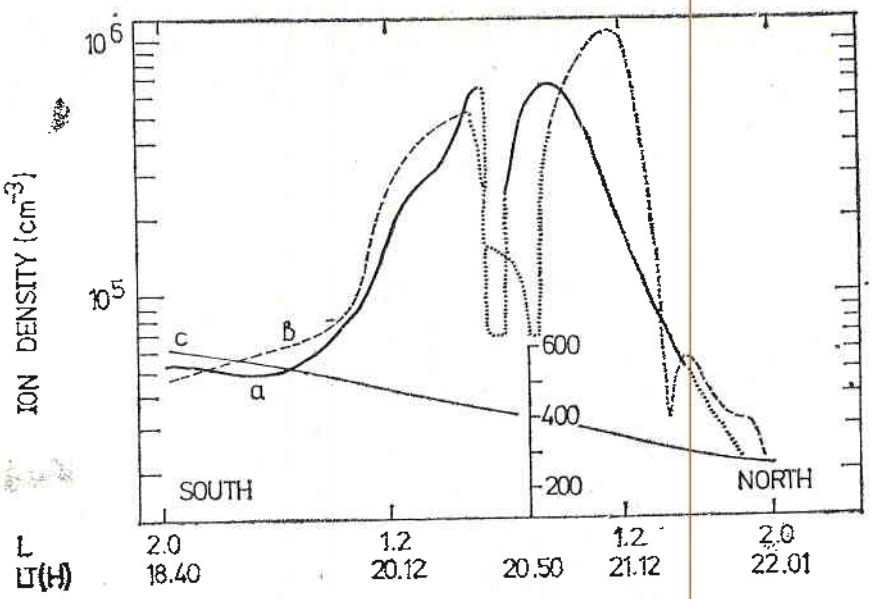

Fig. 10. O^- density obtained in two consecutive orbits of INTERCOSMOS-8
The portions of the curves around the equator drawn by dots show the presence of small-scale irregularity structure. The bottoms of ion depletions in the equatorial region represent the sensitivity threshold of the instrument: *a* — longitude 39°; *b* — longitude 18°; *c* — the average altitude

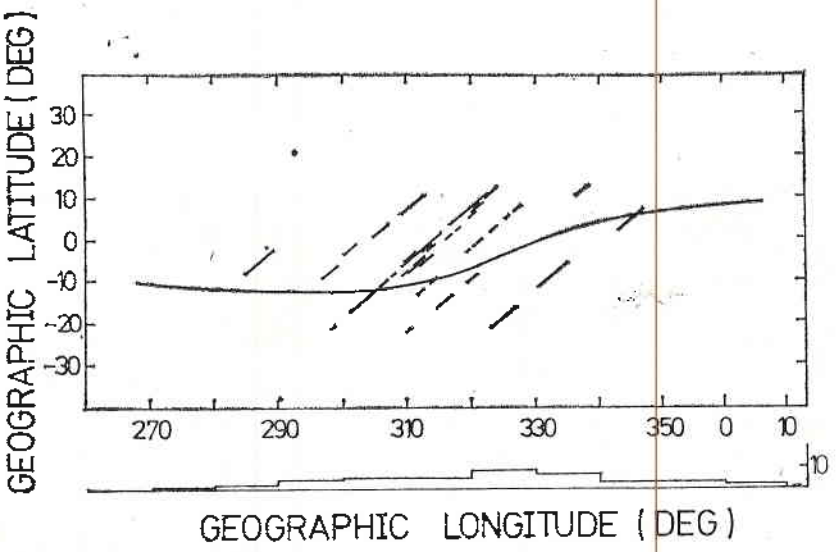

Fig. 11. Geographic distribution of irregularity structure at altitudes of about 1000 km measured by INTERCOSMOS-2 in the winter of 1969, where the dominant ion was H^+. LT 20.00-06.00 h

resolution of the measurements is sufficient to detect irregularities, as low as 2 km in size. The histogram at the bottom of the figure shows the number of transits in each 10° longitude interval used to construct the figure. It is obvious that the probability for the occurence of irregularities is longitude-

dependable. In the region considered the irregularity structure appears between —80° and —20° longitude. As it has been shown above, in this region the transequatorial plasma flow induced by neutral winds is most intensive. It is clear that the irregularity generation is somehow influenced by the interaction

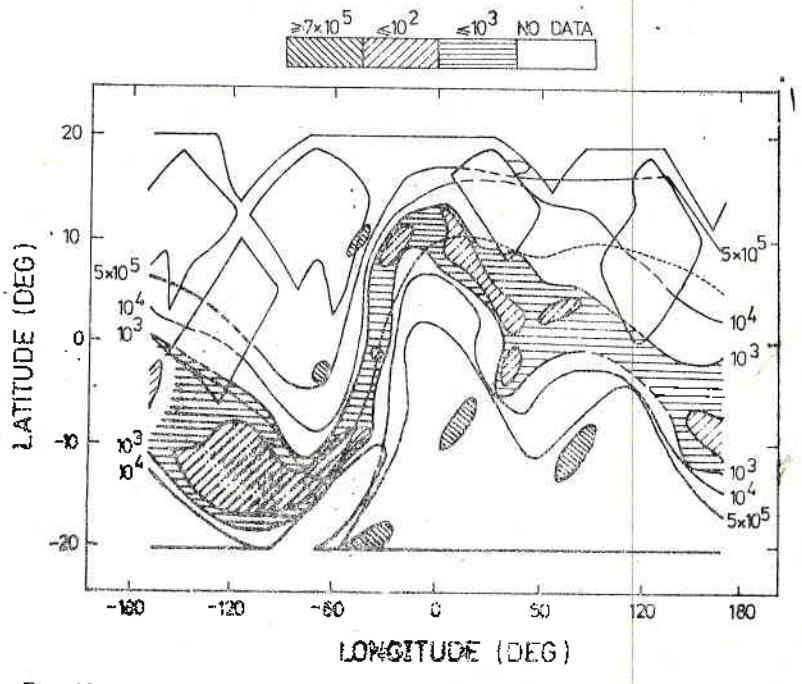

Fig. 12. Contours of O^+ density measured by BIMS on AE-E satellite in the winter of 1977-1978

between neutral winds at the F-region heights and the ionosphere. In [18] large scale plasma irregularities are considered as a result of a direct action of meridional winds over the ionosphere.

Fig. 12 shows the contours of O^+ density measured at 270-320 km between 18 and 24 h local time by Bennet ion mass spectrometer (BIMS) on AE-E in winter 1977-1978. The shaded area marks the regions where O^+ number density below 10^3 cm^{-3} have been recorded. These depletions are placed mainly on the summer side of the equator, being closer to it in the regions with higher magnetic declination. Theoretical contours of the vertical ion drift are shown in Fig. 13. For these calculations simple models of electric field and winds are considered varying only in latitude. Diffusion velocity is calculated for a neutral density of 5×10^6 cm^{-3} at the maximum of F-layer. The comparison of Fig. 12 and Fig. 13 shows an excellent coincidence between the ion drift maximum and the O^+ density minima in the whole of the longitude interval.

Many researchers associate the occurence of irrequlrities in the F-layer with the generation of the so-called 'bubbles' [22, 23]. The bubbles being areas of depleted ion density are generated at the bottom of the F-layer where large gradients of ion density exist [24]. Once generated, the bubbles move upwards almost perpendicularly to the magnetic field lines and can reach heights of 1000 km. Born in a certain magnetic flux tube in the equatorial plane, the

depleted area creates diffusive flows whose magnitude depends on the velocity of the bubbles moving upwards. As a result of this, the total ionization in this particular flux tube can decrease significantly. According to [25], the bubbles create both vertically elongated depletions and depletions along the magnetic

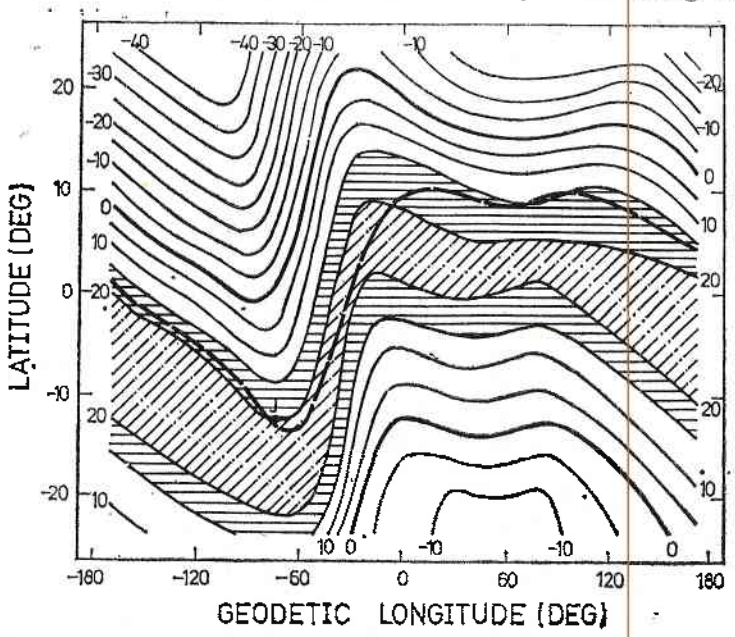

Fig. 13. Contours of vertical ion drift velocity (m/s) calculated under possible winds and electric field conditions in D months
Positive velocity is upwards ; altitude 300 km ; LT 19.00-22.00 h

field lines. Taking into consideration such a complicated structure of ion density distribution, there can be drawn a parallel between Fig. 11 and Fig. 12. There is an impression that they are not so much consistent, although they represent one and the same season in the solar maximum years. A possible explanation might be that the two figures represent different types of irregularities. The INTERCOSMOS-2 data represent small-scale irregularities: 2-5 km in size, while AE-E data reveal large-scale plasma depletions which may not be accompanied by small-scale irregularities. Now it is considered [25] that the bubbles generation is due to, or is accompanied by, strong plasma turbulence which dissipates as bubbles move upwards. At higher altitudes the smaller-scale irregularities get smoothed out due to the large diffusion coefficient. The smaller-scale irregularities appear in Fig. 11 at the region of maximal transequatorial plasma transport. Apart from the highest magnetic declination, the plasma flow over the equator is favoured by the lowest value of L parameter. The latter implies that magnetic force line emerging from the Earth at one and the same geomagnetic latitude will pass over the equator in a region considered by 150 km lower than over the other longitudes. The net plasma flow driven through by neutral winds is most intense in this valley and can elevate irregularities to heights observed in Fig. 11.

Acknowledgement: The author is obliged to Prof. K. Serafimov, Ts. Dachev, L. Bankov and other collaborators from the Central Laboratory for Space Research whose works have been used in this paper.

References

1. Serafimov, K., I. Kutiev, J. Arsov, Ts. Dachev, G. Stanev, G. Gdalevich, V. Afonin, V. Gubsky, V. Ozerov, Ya. Schmilauer. — Space Res., 16, 1976, 27.
2. Serafimov, K., I. Kutiev, J. Arsov, Ts. Dachev, G. Stanev, G. Gdalevich, V. Afonin, V. Gubsky, V. Ozerov, Ya. Schmilauer. — Space Res. in Bulgaria, 1, 1978, 5.
3. Eccles, D., J. W. King. — Proc. IEEE, 57, 1969, 1112.
4. Goldberg, R. A. — Proc. IEEE, 57, 1969, 1119.
5. Anderson, D. N. — Planet. Space Sci., 21, 1973, 409.
6. Goldberg, R. A., P. C. Kendall, E. R. Schmerling. — J. Geophys. Res., 69, 1964, 417.
7. Rush, C. M., S. U. Rush, L. R. Lyons, S. V. Venkataswaran. — Radio Sci., 4, 1969, 829.
8. Chandra, S. — J. Atm. Terr. Phys, 37, 1975, 359.
9. Gdalevich, G. L., B. N. Gorojankin, Ts. Dachev, I. Kutiev, K. Serafimov. — Compt. rend. Acad. Bulg. Sci., 26, 1973, 755.
10. Gdalevich, G. L., B. N. Gorojankin, I. Kutiev, D. Samardjiev, K. Serafimov. — Kosmicheskie Issledovaniya, 11, 1973, 2 (Russ.).
11. Hoffman, J. H., W. H. Dodson, C. R. Lippincott, D. H. Hammack. — J. Geophys. Res., 79, 1974, 4246.
12. Gdalevich, G., B. Gorojankin, Ts. Dachev, I. Kutiev, K. Serafimov. — Bull. Inst. of Geophys., 20, 1974, 39 (in Russian).
13. Gdalevich, G., B. Gorojankin, I. Kutiev, D. Samardjiev, K. Serafimov. — Bull. Inst. of Geophys., 19, 1974, 71 (Russ.).
14. Hanson, W. B., S. Sanatani, D. Zuccaro, T. Flowerday. — J. Geophys. Res., 75, 1970, 5483.
15. Kutiev, I., R. Heelis, S. Sanatani. — J. Geophys. Res., 85, 1980, 2366.
16. Serafimov, K., Ts. Dachev, L. Bankov, I. Kutiev. — Reprint GLSR 8301, 1983.
17. Dachev, Ts., G. C. G. Walker. — J. Geophys. Res., 87, 1982, 7625.
18. Dachev, Ts. Private communication, 1981.
19. Bankov, L., Ts. Dachev. — COSPAR Space Res., 1978, 273.
20. Serafimov, K., Ts. Dachev, I. Kutiev, G. Gdalevich. — Proc. of the Symp. on Magnetospheric Ionospheric Physics. Sun and Solar Wind. Gorbanovo, 1979, 374 (in Russian).
21. Hanson, W. B., S. Sanatani. — J. Geophys. Res., 78, 1973, 1167.
22. Dyson, P., R. Benson. — Geophys. Res., Lett., 5, 1978, 795.
23. Ossakov, S., P. Chaturvedi. — J. Geophys. Res., 83, 1978, 2085.
24. Chaturvedi, P. K. — J. Geophys. Res. 83., 1978, 4219.
25. Tsunoda, R., R. Livingstone, J. P. McClure, W. B. Hanson. — J. Geophys. Res., 87, 1982, 9171.

Внешняя атмосфера на средних и низких широтах

И. С. Кутиев

(Резюме)

Автор делает попытку обобщить некоторые результаты спутниковых исследований средней и нижней ионосферы, проведенных в Центральной лаборатории космических исследований в София за последние 13 лет. Приведены данные о широтной и долготной структуре этой области в свете современных пониманий происходящих в ней процессов и явлений. Отдельно рассматривается поведение околомаксимумной части слоя и области на высоте около 1000 км. Эти две области находятся в контакте и взаимодействии посредством процессов диффузии и обмена зарядами. Рассмотрены долготные особенности в распределении ионной плотности как результат взаимодействия нейтральных ветров при разных конфигурациях магнитного поля. Уделено внимание появлению неоднородностей в экваториальном районе и причине образования неоднородной структуры.

BULGARIAN ACADEMY OF SCIENCES

SPACE RESEARCH IN BULGARIA, 5

Sofia 1986

Space Plasma Emissions — Indicator of Magnetospheric-Ionospheric Processes

M. M. Gogoshev

Introduction

Airglow investigations were initiated at the beginning of this century after the experiments of the English astronomer Simon Nucomb, related with measurements of sky brightness. He was the first to make the conclusion that the sum brightness of stars, galaxy, zodiac light and other sources is not sufficient to interpret the observable night glow. These experiments laid the foundations of a new scientific field, intermediate between astronomy and geophysics. Using mainly astronomical methods orientated to geophysics, the airglow intestigations, especially during the 50s of this century, largely contributed to the more complete understanding of the physico-chemical processes of the so-called 'low-temperature surrounding space plasma.'

We may summarize that this type of measurement provide abundant information on:

1. neutralizing processes in the ionosphere;
2. availability of minor constituents and their distribution into the atmosphere;
3. wide range of aeronomical reactions, their velocities and temperature dependence;
4. interaction between ionized and neutral components;
5. magnetospheric effects on the ionosphere, both in auroral and at mid- and low latitudes.

These studies provide important information on many other processes and phenomena which cannot be efficiently investigated mainly through the classic radiophysical methods. Fig. 1 illustrates a general diagram of the solar energy transformation (irradiation and particles) into a glow as a finite product [25].

The Bulgarian contribution to the airglow studies started with K. Serafimov's theoretical works in the 60s [1, 2. 3]. They were substantially devoted to the interpretation of the green oxygen line behaviour and mainly to its aroundmidnight maximum.

The first experimental observations and the initiation of systematic, various airglow investigations in Bulgaria had started later, in 1968 [4]. Different types of photographic and electrophotometric instruments were developed at the

Observatory of Stara Zagora. Various techniques for spatial and spectral study of the optical emissions were developed here along with stationary airglow facility [5] successfully used not only in the Bulgarian observatories, but also in India [6], Cuba [7] and Guinea, Konakry [8].

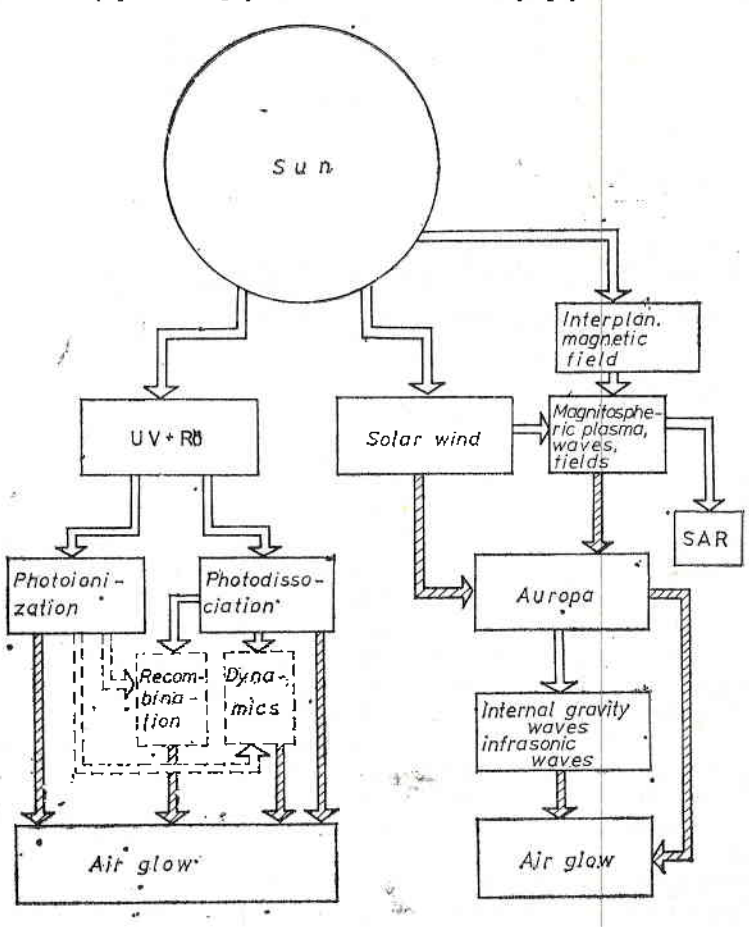

Fig. 1. Scheme of the dissipation of solar energy in the upper atmosphere

The first Bulgarian airglow instrument was launched into space in 1977 This was an electrophotometer aboard the VERTICAL-6 rocket, developed for the measurement of the vertical profiles of various optical emissions [9]. Successful experiments were carried out on VERTICAL-7 and 10 and on the two Indian rockets CENTAUR-II B [10].

A 6-channel electrophotometer was launched aboard INTERCOSMOS-19 in February, 1979 to measure the main spectral emissions in the upper atmosphere in the visible spectral range.

Successful experiments were carried out with tilt filter photometers, operated by cosmonauts aboard SALYUT-6 and SALYUT-7 stations. These studies, along with the various optical experiments aboard the INTERCOSMOS-BULGARIA-1300 satellite, launched on August 7, 1981, substantially contributed to the understanding of the physical processes in the surrounding space plasma, some of which will be discussed here.

Airglow and nighttime F-region behaviour

Some scientists had originally concluded in the 40s that the behaviour of the red oxygen line with a wavelength of 630 nm correlated with some parameters of the nighttime F-region of the ionosphere. Nevertheless, only at the beginning of the 50s D. Barbier [11] suggested a semi-empirical formula for the relationship between the measured integral intensity of the emission and the F-layer height and its critical frequency. This formula has the form of:

$$I_{630} = K(f_0F)^3 e^{-\frac{h'F-200}{H}} + C. \tag{1}$$

Here K and C are two constants, depending both on the situation of the observational station and on the concrete observation conditions. On the basis of a more advanced theory for the ionospheric processes in the F-layer and assuming that:

a) the main generative mechanism of λ 630 nm during nighttime is the dissociative recombination of the O_2^+ ions;

b) they are obtained through exchange reactions between O^+ and O_2;

c) the density of O_2 beyond 200 km varies after the exponential law;

d) the electron density around the layer maximum is approximated by a parabolic function, and above this by an exponential, Serafimov and Gogoshev have obtained [12, 13] a much more accurate dependence than Barbier, where part of the empirical constants acquire also physical content. This is as follows:

$$I_{630} = K_C(f_0F)\varphi(H, Z_m)e^{-\frac{h'F-200}{H}} + C. \tag{2}$$

Here, similar to (1), the critical frequency of the F-layer is denoted by f_0F, $h'F$ being the virtual height of the F-layer, H is the scale height of the neutral atmosphere and $\varphi(H, Z_m)$ is the function describing the geometry of the F-layer.

Very important result is the fact that the constant K of Barbier's formulae acquires the following physical meaning

$$K_C = 1.24 \cdot 10^4 K_{exc} [O_2]_{200}, \tag{3}$$

where K_{exc} is a constant of the velocity of the exchange reaction $O^+ + O_2 \rightarrow O_2 + O$ and $[O_2]_{200}$ is the oxygen molecules density at a level of 200 km. Obviously, when through a series of experimental observations on I_{630} the numerical value of K_C is determined, then it is possible to obtain such an important parameter as $[O_2]_{200}$.

Investigations on topside F-layer portion through optical emissions

Few are the optical emissions, irradiated into the topside F-region. Two of the most substantial are the oxygen λλ 130,4 nm and 135,6 nm. Situated into the region of the so-called vacuum ultraviolet, they are inaccessible to direct measurements from the earth surface. Regardless to this, their great informability was demonstrated in the few rocket and satellite experiments performed.

Serafimov devoted series of theoretical publications [14-17] to the theory of excitation and glow of these two spectral lines. Further, this fundamental

theory was accompanied with various experimental works, based on direct measurements of the intensity of the two lines aboard the INTERCOSMOS-BULGARIA-1300 satellite [18-21].

Serafimov assumes the following generative mechanisms into the analysis of the λ 130,4 nm excitation:

a) radiative recombination of O^+ ions with electrons;

b) ion recombination of positive and negative atomic ions in the F-region (O^+ and O^-);

c) collision excitation by soft electrons (of energies above 9 eV).

Most productive of these mechanisms is the first one, occuring in the topside F-region.

Each of these generative mechanisms, the regions of predominant effect of each versus the others and their quantity values were estimated by Serafimov in his works. He founds in [22] the following complete expression for the bulk velocity of the emission of $I_{130,4}$ into the F-region of the ionosphere

$$\frac{dI_{130,4}}{dh} = C_{130,4}K_q\left\{\alpha_{e,1304}\cdot N_e\cdot[O^+]+\alpha_{i,130,4}\cdot[O^-]\cdot[O^+] + \int_g^{E_r}\sigma_{130,4}\cdot B\cdot N_e\cdot e^{-P_1Ee}\,dEe\right\}, \tag{4}$$

where K_q is the quenching coefficient of deactivation of the excited oxygen term; $\alpha_{e_1\,130,4}$, $\alpha_{i,\,130,4}$ are the velocity constants of the radiative and ion recombinations of O^+ with electrons and O^-ions, respectively, $\sigma_{130,4}$ is the cross section of the electron collision of O with electrons at output $O(2p^33s^3S_1^0)$; E_r is the upper boundary of the integral by energies which in Serafimov's opinion may be sufficiently assumed up to 100 eV; P_1 is an index in the exponential of the electron flux spectrum, BN_e is the amount of electrons from the flux of energy $E_0=9$ eV, wherefrom the excitation of the triplete around λ 130 nm starts with electron collision. Serafimov found complete expression for the emission vertically (zenith intensity) of λ 130,4 nm integrating by the height h, under approximations of the altitudinal distribution of the subintegral functions deduced by him. This expression is to be properly compared with the experimental data.

Successfully using the models for the neutral components distribution into the upper atmosphere, Serafimov considered the increase of λ 130,4 nm intensity due to its multiple resonance scatter from the atmospheric components. In the result to this the observable intensity of λ 130,4 nm depends on the height of the satellite, and of the UV instrument, respectively. This effect is significantly reflected on the measured ratio of $I_{130,4}/I_{135,6}$ which will be discussed further on.

Similar procedure was made to analyse the other ultraviolet emission of a length λ 135,6 nm. Serafimov defined that the output term $O(2p^33S^5S_1^0)$ of this emission had the same generative mechanisms as that of λ 130,4 nm [23]. Similar to (4) is the expression for the bulk velocity of λ 135,6 nm emission.

Serafimov obtained for the bulk velocity of emission for both lines

$$\frac{\frac{dI_{135,6}}{dh}}{\frac{dI_{130,4}}{dh}} = \frac{\varphi_1(h)N_e+\int_g^{E_r}\sigma_{135,6}\,B_1\,e^{-P_1E_e}\,dE_e}{C_{1304}(h)\left[\varphi_2(h)N_e+\int_g^{E_r}\sigma_{130,4}\,B_1\,e^{-P_1E_2}dE_2\right]}. \tag{5}$$

$\varphi_1(h)$ and $\varphi_2(h)$ in this expression are linear functions of $\alpha_{e_1\,135,6}$ and $\alpha_{e_1\,130,4}$ of $R_e=\frac{[O^+]}{N_e}$ and of $\lambda_0=\frac{[O^-]}{N_e}$.

The examination of the bulk velocity ratio was not accidental, since as we have shown above, the zenith intensity of λ 130,4 nm depends on the distribution and density of neutrals, as well as on the area of the emitting region.

Global diagnostics of ionospheric parameters through optical data only

Bittencourt and Tinsley were the first [24] to draw attention to the fact that the intensity of the red oxygen line is very sensitive and depends on the height at which is located the maximum of the nighttime F-layer. Simultaneously, similar is the behaviour and the dependence on the maximum electron density of λ 135,6 nm. The authors were the first to suggest the idea to diagnose the specifically important parameters h_mF and N_mF through the combined measurements of these two lines.

Based on the thorough studies of λ 630 nm and of the two ultraviolet lines λλ 130,4 nm and 135,6 nm made by the Bulgarian scientists, K. Serafimov suggests a more complete and correct interpretation of the combined use of the two airglow emissions for the determination of these important ionospheric parameters [17]. While Bittencourt and Tinsley used semiempirical dependence for the determination of the $I_{135,6}$ dependence on N_mF, Serafimov defines the same based on formulae deduced by him for $I_{135,6}$ emission and with the use of the international reference models IRI. The latter are used to give the shape of the profile only, while the maximum value of the electron density N_mF is given by the measured $I_{135,6}$. This dependence is as follows:

$$(6)\qquad I_{135,6}=1{,}19\,.\,10^{-12}\,A_0\,.\,A_1^2(N_mF)^2e^{-PA_0}\left(\frac{e^{-PA_0}}{S}-\frac{e^{-PA_0X_2}}{5X_2^5}\right.$$

$$-\frac{PA_0}{20}\left\{e^{-PA_0}-e^{-PA_0X_2}\left[1-PA_0\left(\frac{1}{3X_2^2}-\frac{PA_0}{6X_2^2}+\frac{P^2A_0^2}{6X_2}\right)\right]-PA_0e^{-PA_0}\left[\frac{1}{3}-\frac{PA_0}{6}\right.\right.$$

$$\left.\left.+\frac{(PA_2)^2}{6}\right\}+\frac{(PA_0)^4}{6}\left[E_1(-PA_0X_2)-E_1(-PA_0)\right]\right).$$

In this rather long, but very suitable for computation expression, the parameters A_0, A_1, A_2 and P are taken from the IRI models for each concrete case, $X_2=1+\frac{h-h_m}{A_0}$, and E_1 is generally adapted denomination of the intgral-exponential function.

Formula (6) in combination with h_mF determined through λ 630 nm measurements, enables the determination of N_mF practically in any point above the earth surface, through the use of a relatively cheap and accessible satellite technique, i. e. with the incorporation of optical equipment. (Here the alternative possibility is considered — the use of a satellite ionosonde — a very expensive technique).

Verification of compatibility of neutral and ionospheric models through airglow observations

As it is known, the first models for the distribution of the neutral components in the upper atmosphere were built up at the beginning of the 60s (UR standard atmosph., CIRA-55, Jacchia-71, etc.). Data mainly from the measured satellite resistance were used for the purpose, resulting from shortening of the satellite orbit and from mass-spectrometric data, too. These models were improved regularly and after CIRA-75 and Jacchia-77, the most precise one at the moment is the MSIS model.

The ionospheric models composed by Prof. Rawer's group within the scope of COSPAR and URSI were initiated in 1975 [27]. They are also subject to continuous improvement.

Many experiments on the simultaneous use of neutral and ionospheric models for practical geophysical computations have shown certain incompatibility and necessity of improvement. Many Bulgarian publications of Serafimov, Gogosheva, Gogoshev and others revealed a very accurate criterion for such compatibility [26, 28, 29]. The excitation and the emmission of the red oxygen line is used for the purpose — λ 630 nm in nighttime ionosphere. Many studies, including Bulgarian, have shown that in a calm geomagnetic situation the following aeronomic reactions are basic for the formation of λ 630 nm at night-(time of the F-region

(7) $$O^+ + O_2 \rightarrow O_2^+ + O;$$

(8) $$O_2 + e \rightarrow O(1_D) + O(3P).$$

The first of these reactions (7) is limiting to the emission velocity. Here the ion component (O^+) participates in ion-exchange reaction with the main neutral O_2. Thus, we may write the following expression for the exchange velocity of emission:

(9) $$\frac{dI_{630}}{dh} = \frac{\varepsilon_1 A_{630} \gamma_1 N_m F \cdot S(h)}{A\left[1+\frac{d(h)}{A}\right][1+B(h)]}.$$

In this formulae, ε_1 is the quantum output of reaction (8); recent satellite measurements yield $\varepsilon_1 \approx 1{,}33$; $A_{630} = 0{,}069\ s^{-1}$; $A = 0{,}0091\ s^{-1}$; $S(h)$ is profile-shaping factor; $N_m F S(h) = N_e(h)$ is the local electron density, and $d(h)$ and $B(h)$ are the deactivation factors, depending also on the altitudinal distribution of the neutrals. Through the integration of the two sides of equation (9) by the height h we obtain a dependence of the column emission (zenith intensity) in dependence of the distribution of N_e and O_2 with the height. The latter are taken from IRI and any neutral model, respectively. Experimentally comparing the measured zenith intensities with the theoretical values thus defined, the compatibility of ion and neutral models is estimated.

In the publications of Serafimov and others a thorough study is made on comparison between theory and observations on the nighttime emission of λ 630 nm, performed in the observatory of Stara Zagora. It is found that the model computations give intensities at midnight of the order of several Reileighs for low solar activity, while the actually measured ones are 20-30 R. The use of various neutral models (for example Jacchia-77 and MSIS) and IRI provide the same results. This fact, as well as some other criteria, contributed to the conclusion that the IRI-models at low solar activity should be corrected, since the electron density deduced by them is lower than the actual one.

Conclusion

The study of the optical emissions in the last decade contributed significantly to the clarification of the sophisticated complex of solar-terrestrial interaction as a whole, and of the magnetospheric-ionospheric processes in particular. A lot of Bulgarian publications — theoretical and experimental — ground-based, rocket and satellite, contributed to the more thorough penetration and study of the energy transfer in the surrounding space environment, which together with its fundamental nature is of definite practical importance.

References

1. Serafimov, K. B. — Gerlands beiträge zur Geophysik, 73, 1964, 1.
2. Серафимов, К. Б. — Изв. Геофиз. инст. БАН, 4, 1963, 151.
3. Серафимов, К. Б. Светене на нощното небе. — Природа, 1966, 1, 14.
4. Гогошев, М., К. Серафимов. — Изв. Геофиз. инст. БАН, 17, 1971, 17.
5. Gogoshev, M., S. Chapkunov. — Space Res. in Bulg., 1, 1978, 73.
6. Murty, G. S. N. Some Upper Atmosphere Studies Using the Ground-Based Night Airglow Measurements. — P. H. D. Thesis, Andhra Univ., India, 1973.
7. Gogoshev, M., S. Chapkunov, J. Gonzales, L. Palasio, G. Hill. — Space Res. in Bulg., 2, 1979, 24.
8. Гогошев, М., С. Чапкънов. — Геомагнетизъм и аерономия, 17, 1978, 164.
9. Gogoshev, M., St. Sargoichev, Ts. Gogosheva, K. Kazakov, B. Taneva, I. Mendev. — In: Low Latitude Aeron. Processing, COSPAR series, 8, 1979, 297.
10. Gogoshev, M., K. Serafimov, N. Petkov, St. Sargoichev, Ts. Gogosheva. — Bulg. Geophys. J., 5, 1979, 22.
11. Barbier, D. — In: Geophysique exterieure, New-York-London, 1963, 182.
12. Serafimov, K., M. Gogoshev. — Compt. rend. Acad. Bulg. Sci., 25, 1972, 197.
13. Серафимов, К., М. Гогошев. Теория на излъчването на червената кислородна линия в Ф-областта на йоносферата. — Доклади на юбил. научна сесия в Стара Загора, 1971.
14. Серафимов, К. — Бълг. геофиз. спис., 6, 1980, 25.
15. Серафимов, К. — Бълг. геофиз. спис., 7, 1981, 21.
16. Serafimov, K. — Compt. rend. Acad. Bulg. Sci., 33, 1980, 917.
17. Серафимов, К. — Космические исследования. Москва, 20, 1982, 736.
18. Gogoshev, M., K. Serafimov, I. Mendev, S. Sargoichev. — Compt. rend. Acad. Sci. Bulg., 35, 1982, 1069.
19. Gogoshev, M., St. Sargoichev, B. Mendeva, J. Mendev, L. Simeonova, T. Perevodchikova. — Compt. rend. Acad. Bulg. Sci., 36, 1983, 201.
20. Serafimov, K., M. Gogoshev, Ts. Gogosheva. — Bulg. Geophys. J., 9, 1983, 22.
21. Gogoshev, M., B. Taneva, I. Mendev, S. Spasov. A Collection of Upper Atmosphere UV Airglow Spectra, Obtained by IC-Bulgaria-1300 Satellite. Preprint No. CLSR-83-02, Aug., 1983.
22. Serafimov, K. — Compt. rend. Acad. Bulg. Sci., 36, 1983.
23. Serafimov, K. — Bulg. Geophys. J., 7, 1981, 21.
24. Tinsley, B. A., J. A. Bittencourt. — J. Geophys. Res., 80, 1975, 2337.
25. Gogoshev, M., K. Serafimov. Airglow and Ionosphere. (in print).
26. Серафимов, К., М. Гогошев, Цв. Гогошева. — Геомагнетизъм и аерономия, 17, 1977, 1044.
27. Rawer, K., S. Ramakrishnan, D. Bilitza. Preliminary Reference Profiles for Electron and Ion Density and Temperature (IRI). — IPW-Sci. Rep., W. B. 2, 1975.
28. Gogosheva, Ts., K. Serafimov, M. Gogoshev, S. Spasov. Optical Testing of IRI and MSIS Intercomparison. — Paper, presented at the XXII COSPAR Mtg., Budapest, 1980.
29. Serafimov, K., M. Gogoshev, B. Taneva, Ts. Gogosheva, I. Mendev, Ts. Pashova. — Compt. rend. Acad. Bulg. Sci., 32, 1979, 1343.

Излучение космической плазмы — индикатор магнитосферно-ионосферных процессов

М. М. Гогошев

(Резюме)

Сделан обзор основных физико-химических процессов, протекающих и приводящих к возбуждению и излучению оптических эмиссий в космической плазме. Исследование этих излучений даст важную информацию о нейтрализационных и ионизационных процессах, о скоростях аэрономических реакций, о плотностях малых составляющих, о взаимодействии ионизированных и нейтральных компонент, о воздействии магнитосферы на ионосферу Земли. Конкретно показано участие болгарских ученых в этих исследованиях, начавшихся работами К. Серафимова с начала 60-х годов. Подробно рассмотрены результаты излучения надмаксимумной части F-области при помощи оптических эмиссий, а также улучшения международных ионосферных и нейтральных моделей и диагностики магнитосферно-ионосферных связей.

BULGARIAN ACADEMY OF SCIENCES

SPACE RESEARCH IN BULGARIA, 5

Sofia . 1986

On Measuring Instruments for Space Plasma Electron Component Parameters in the Presence of 'Plasma-Body' Potential Difference

S. K. Chapkunov

The measuring instruments for space plasma electron component parameters are applied in the study of the surrounding space aboard artificial earth satellites when variable potential is available at the space object (satellite body).

Such instruments are familiar from reference sources as performing experiments with the help of Langmuir cylindric probes [1, 2, 3]. They are composed of a current-voltage converter (TCV), connected with the cylindric probe collector (CSL). In turn the TCV output is connected with the telemetric system (TMS), as well as with sawtooth voltage generator (GSTV). The latter controls the protective electrode of the CSL.

The disadvantage of the described instruments is incomplete measurement of space plasma electron component parameters (only density or electron temperature in restricted range) under relatively high potential of the body with respect to the surrounding environment of plasma. Complete loss of information is to be observed occasionally in such experiments.

I. In order to design instruments for measurement of plasma electron component parameters with CSL so as to obtain complete scientific information on the density and the temperature of the electrons in the direct measurements aboard the spacecraft within a large range of variation of the body-plasma potential difference, it is necessary to satisfy several conditions.

First, it is necessary to incorporate an additional system for automatic control of the variation range of the sweep voltage, applied to the electrodes of the CSL, in dependence on the value of the mentioned potential difference. In general, this system contains a TCV converter, connected with the collector and the protective probe electrode. The TCV output transports the converted and enhanced signal to the TMS, as well as to the system for automatic selection SAC of the translation voltage. One of the outputs of SAC is controlled by the probe protective electrode and the other is connected with the TMS. The other input of the SAC controls the output of the main generator GSTV.

Such a device has positively advantages as compared with systems now in use.

An examplary design of the described instruments is given in Fig. 1 where *1* — is probe (protective electrodes); *2* — potential meter; *3* — DC-, DC voltage converter; *4* — collector of cylindric probe; *5* — second converter of DC-DC voltage; *6* — input (output of amplifier-differentiator); *7* —

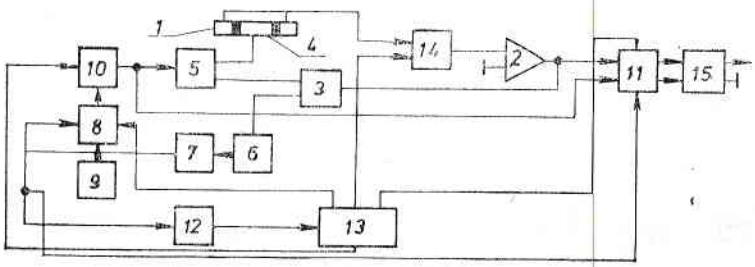

Fig. 1. An example of a block diagram

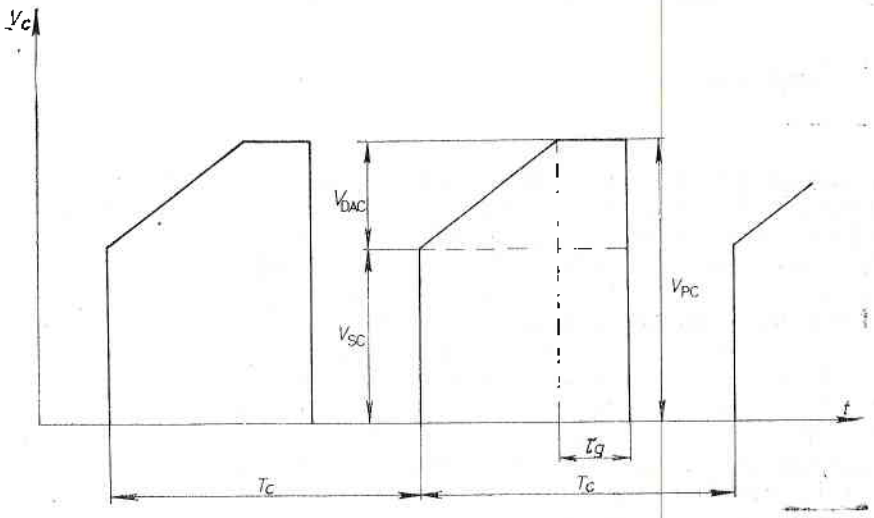

Fig. 2. An example of a time-voltage diagram

peak detector; *8* — first switch; *9* — pulse generator; *10* — digit-to-analog converter; *11* — second switch; *12* — retarding block; *13* — 'measurement sampling' block; *14* — switch; *15* — analog summator.

The principle of performance is the following: the protective electrodes of the cylindric Langmuir probe, in fact 'floating' (insulated from the body and the other equipment), are charged to potential V_{SC}, close to the potential of the surrounding plasma V_{PC}. At the initial phase of each measurement cycle one of the inputs of the switch *11* is closed by block *13*, and switches *8* and *14* are open. The collector *4* receives initial potential V_{SC} from the output of the potential meter *2* after conversion into convertor *3*, equal to the potential of the protective electrodes *1*. Through the closed switch *8* at the input of the digit-to-analog converter, pulses from generator *9* are fed in the result of which linearly changing voltage V_{DAC} is generated at the output of converter *10*. This voltage after being converted into converter *5*, is added to the voltage at the output of the first converter *3* and changes the potential of collec-

tor *4* [4]. Due to the serial connection of blocks *5*, *3*, *6* to collector *4*, a signal is obtained at the output of amplifier-differentiator *6*, which is proportional to the derivative of the collector current i_k in time $\frac{dI_k}{dt}$. Since the variation law of the potential of collector *4* in time is linear, the signal is proportional also to the derivative $\frac{dI_k}{dU_k}$. This performance is interpreted with the following theoretical consideration: the volt-ampere characteristics of the probe are composed by two sectors of different curvature. The potential of the collector in the inflextion point of this curve is identified with the potential of the surrounding plasma. At the moment when this derivative attains its maximum, a signal occurs at the output of the peak detector *7*, which opens switch *8* and provides resolution to switch *11*. The determined value of the signal from the output of the digit-to-analog converter *10* is summed in the analog summator *15* with the value of the potential difference V_{CK} between the 'floating' electrodes *1* and the body from the output of meter *2*. At the output of summator *15* we obtain potential equal to the plasma-body potential difference.

The signal from the first detector *7*, after certain delay T_D determined by the retarding block *12*, is fed to 'measurement sampling' block *13* which closes switch *11* and repeats the measurement cycles of periodicity T_C.

II. All the things discussed thus far could be summarized and specified, considering the fact that the bulk charge generated as a rule depends on the size of the radius of Debay, and hence, on the measurement height. In addition, the consideration of the error in the measurement is not possible without some other additional probe measurements. The aim of the following analysis is to consider the effect of the bulk charge arround the probe and as a result to decrease the errors in probe applications of space experiments. This problem is resolved as follows (Figs 3 and 4). Fig. 3 illustrates the block diagram of the discussed instrument and Fig. 4 shows the temporal diagrams of the instrument (in particular to the outputs of the two generators of trapezoidal voltage -- blocks *4* and *5*).

The principle of performance is the following: each cycle of performance on the diagram contains four characteristic time intervals respectively denoted by t_1, t_2, t_3 and t_4. The ratios $t_1+t_2+t_3<t_4$ and $t_1=t_2\gg t_3$ are valid for them. During t_1 the block controls the logics *7*, switches through switch *3* the second end electrode *1* to the collector of probe *2*. The cylindric Langmuir probe performs as a unilateral protected probe of length $l=l_{(1)}+l_{(2)}=2l_{(2)}$ in total. The current from the collector (already 1+2) it converted into voltage by current-voltage converter *6*, and the latter is fed to integrator *10* through switch *8* and the first (upper) channel of distributor *9* where it is memorized. During the period t_1+t_2 the second end electrode *1* is switched by block *7* through switch *3* to the first end electrode *1* and the probe operates as a bilateral protected Langmuir probe with collector length of *l* [5]. The current from collector *2* is transformed into voltage by *6* and through second switch *8* and second channel of distributer *9* is fed to the input of integrator *11* where it is memorized. During the interval of $t_1+t_2+t_3$ the generator *5* generates dc voltage of value equal to the maximum accelerating voltage of the linearly decreasing sweep. During t_1+t_2 switches *12* and *13* are closed open. During t_3 switches *12* and *13* are closed and the voltages from the outputs of integrators *10* and *11* are fed to the inputs A and B of summator *14*, as channel A has coefficient of convergence "1" and channel B has coefficient of convergence "2". At the output of summator *14* we obtain voltage, proportional to the

current, determined by the availability of the bulk charge in the frontal part of the second end protective electrode *1*.

During t_4, switch *3* switches second end electrode *1* in its capacity of protection (1+1). The current of collector *2* is transformed by *6* into voltage

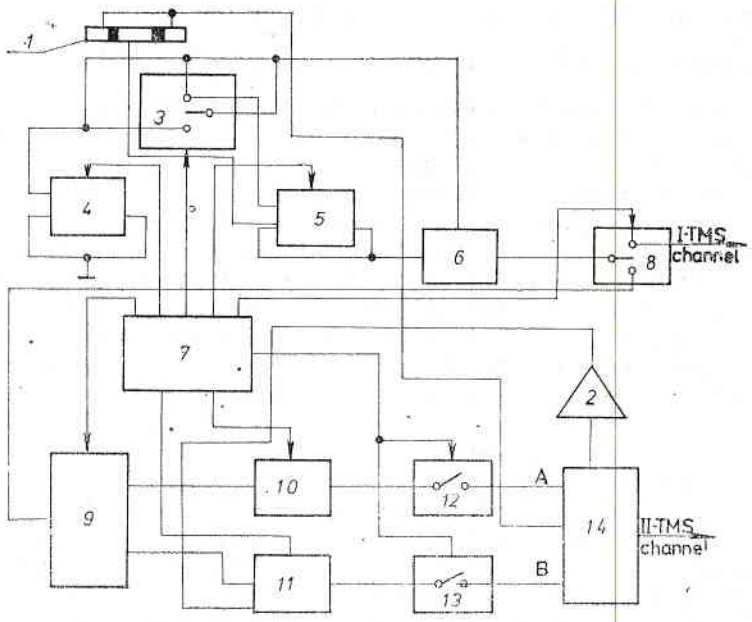

Fig. 3. The actual block diagram of the device

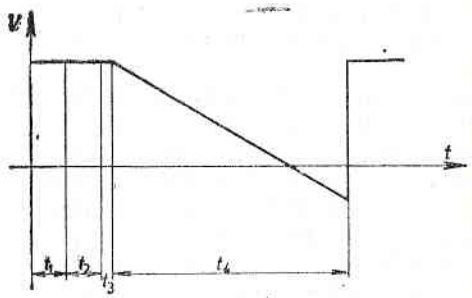

Fig. 4. Temporal diagrams of the instrument

and the latter is fed to the I telemetric channel through switch δ. During t_4 the second generator operates in linear decreasing sweep mode (Fig. 4).

The output signal obtained in the interval t_4 describes the volt-ampere characteristics of the probe, and the electron density is computed by its slope, through the use of familiar formulae of plasma theory. The signal obtained within interval t_3 is determined by the availability of bulk charge and contains information on the introduced error.

Conclusion

Future attempt will join together the above-mentioned aspects from the minimization, optimization and updating of the probe technique, applying cylindric Langmuir probes in space experiments. It should be mentioned here that in some space experiments in particular the ionospheric-magnetospheric project INTERCOSMOS-BULGARIA-1300 instruments were designed on the basis of the above considerations. They successfully performed and provided abundant information for the fine structuring of the electron plasma component.

The instruments described have been part of the Bulgarian participation in the VERTICAL program.

Acknowledgements: The author is grateful to the entire team of the 'Space Instrumentation' scientific branch, led by him, for their hard work and important consultations during the application of the above-described instruments. He also extends his thanks to Academician Serafimov for his overall support and stimulating guidance in his capacity of Director of the Central Laboratory for Space Research at the Bulgarian Academy of Sciences.

References

1. Findley, J. A., L. H. Brace. The Cylindrical Electrostatic Probes Employed on Alouette II and Explorer XXXI Satellites. — PIEEE, 57, 1969, 1054-1056.
2. Brace, L. H., R. F. Theis. The Behaviour of the Plasmapause at Mid-Latitudes ISIS-I Langmuir Probe Measurements. — J. Geophys. Res., 79, 1974, 13, 1871-1884.
3. Brace, L. H., R. F. Theis, A. Dalgarno. The Cylindrical Electrostatic Probes for Atmosphere Explorer-C, -D and -E. — Radio Sci., 8, 1973, 4, 341-448.
4. Чапкънов, С. К. и др. Устройство за определяне потенциала на космическа плазма. — Авт. свидет. № 27708/11. 09. 1978 г.
5. Чапкънов, С. К. и др. Цилиндрична сонда за измерване на електронна концентрация. — Авт. свидет. № 26181/31. 03. 1978 г.

Об устройствах измерения параметров электронной компоненты космической плазмы при наличии разности потенциалов „объект — плазма"

С. К. Чапкынов

(Резюме)

Дискутируется ситуация вокруг объекта — носителя научной аппаратуры в реальных условиях. Наличие разности потенциалов „объект — плазма" может привести к ошибочным научным результатам, особенно что касается зондовых методов. В работе сделана попытка описать устройства измерения параметров электронной компоненты плазмы с помощью цилиндрического зонда Лэнгмюра, посредством которых получается полная научная информация о концентрации и температуре электронов при непосредственном измерении с борта КА (в широких пределах изменения разности потенциалов „корпус — плазма"), а также анализировать влияние объемного заряда вокруг зонда и в результате — уменьшить ошибки при применении зонда в космическом эксперименте.

BULGARIAN ACADEMY OF SCIENCES

SPACE RESEARCH IN BULGARIA, 5

Sofia . 1986

The Ceodetic Experiment of the Satellite INTERCOSMOS-BULGARIA-1300

*N. I. Georgiev, A. G. Massevich**

Bulgarian Academy of Sciences,
Central Laboratory for Geodesy —
Sofia
**Academy of Sciences of the USSR,*
Astronomical Council — Moscow

On August 7, 1981, within the framework of the INTERCOSMOS international programme of space research, an artificial earth's satellite INTERCOSMOS-BULGARIA-1300, dedicated to the 1300th anniversary of the Bulgarian State, was launched into the space.

Although the satellite INTERCOSMOS-BULGARIA-1300 was not specifically designed for geodynamic and geodetic studies, it was supplied with a system for laser location. This was the first satellite of this type, since due to their significant weight and dimensions such systems were so far installed on specialized satellites only. Firm restrictions on the weight and dimensions of the laser tracking systems were imposed already in the design stage, since apart from the OLSS system (optical laser light-reflecting system), 11 other instruments were to be housed aboard the satellite. Throughout two years of intensive efforts (1979-1980) this difficult task was successfully resolved in the Central Laboratory for Geodesy at the Bulgarian Academy of Sciences [1,2]. A reflective system of 4,5 kg weight was designed for the satellite, using its very good and stable orientation on the vertical and circular orbit. The shape of a tetrahedral truncated pyramid was selected due to size restrictions, and 12 prisms were located at the small base, 16 at the lateral faces, and the large base was used to fix the system at the satellite bottom. Such an angle was selected between the lateral faces and the base so as to ensure the energy of the reflected signal by the retroreflectors of the base up to zenith angles of $Z=35°$, and at a larger angle up to $Z=\pm 55°$ by the lateral panels. Due to this configuration of the retroreflectors dead zones up to 20% of the circular view occur at $Z=35°$. In order to improve the performance of the OLSS system at the extreme angles of tracking, tripleprisms of coverage and of different divergence were used. The experimental tests on the reflectance capacity of the system, made conjointly by the Central Laboratory for Geodesy and the Astrocouncil of the Soviet Academy of Sciences, had shown that the OLSS system provides a sufficiently powerful signal, up to $Z=60°$, and that the dead

Table 1

Maxim. errors (m)	Duration of tracking interval			
	1 day	7 days	14 days	1 month
Along the orbit	7,4	364	1460	6690
range	5,3	262	1050	4820

Table 2

Interval of observations (MJD)	Epoch of the observations (MJD)	Number of points in the series	Number of points with 50 m	Tracking stations	Mean motion $(n)\frac{\text{rotat.}}{\text{day}}$	Empirical atmosph. coeff. $\left(\frac{n}{2}\right)\frac{\text{rotat.}}{\text{day}}$
44833 —44837	44833.91	160	156	Riga Simeiz	14.138376	5.83E-6
44836 —44840	44836.95	164	163	Potsdam Riga Simeiz	14.138412	9.42E-6
44846 —44850	44846.93	31	27	Potsdam	14.138639	6.33E-6
44850 —44855	44850.89	80	67	Potsdam Riga Zvenigorod	14.138691	10.85E-6
44869 —44875	44869.72	247	214	Riga Simeiz Zvenigorod	14.139016	8.71E-6
44875 —44883	44875.73	245	245	Simeiz	14.139155	6.17E-6
44884 —44890	44886.70	136	136	Potsdam Riga	14.139243	3.54E-6
		1063	1008			

zones made up 17 % of the circular view. The observations, made by 12 laser tracking stations, had confirmed this experiment.

The satellite BULGARIA-1300 is subject to atmospheric drag, in spite of its comparatively high altitude 850 km. This is caused by the considerable size of the solar batteries and by the fact that the satellite was in orbit during a period of high solar activity. Unaccountable fluctuations of atmospheric density could therefore influence the accuracy of determination of the orbital elements.

Possible errors (due to the fluctuations of density not taken into account) of the determination of the satellite position along the orbit and on the slant range are shown in Table 1. These values are determined by the consistent square polynomial method [3] on condition that variations of density are distributed in the worst possible way.

Laser observations of the satellite from four stations — Riga, Simeiz, Zvenigorod, Potsdam — have been processed at the Astronomical Council for estimation of the atmospheric influence on the speed of the satellite motion during the first two months when large splashes of solar activity were observed (Table 2).

One passage a day was observed at each station, if meteorological conditions permitted. Observations were united in series of 5 days. The analytic theory of satellite motion used for the calculations provided an accuracy of the orbit determination at a 5-day interval no better than 50 m. The discrepancies

between measured and computed ranges, after average orbital elements based on all series of observations have been determined, are less than 50 m. The mean value of the average motion (n) and the atmospheric coefficient $\left(\frac{\dot{n}}{2}\right)$ were computed for all arcs. The variations of the index of solar activity F 10.7 and

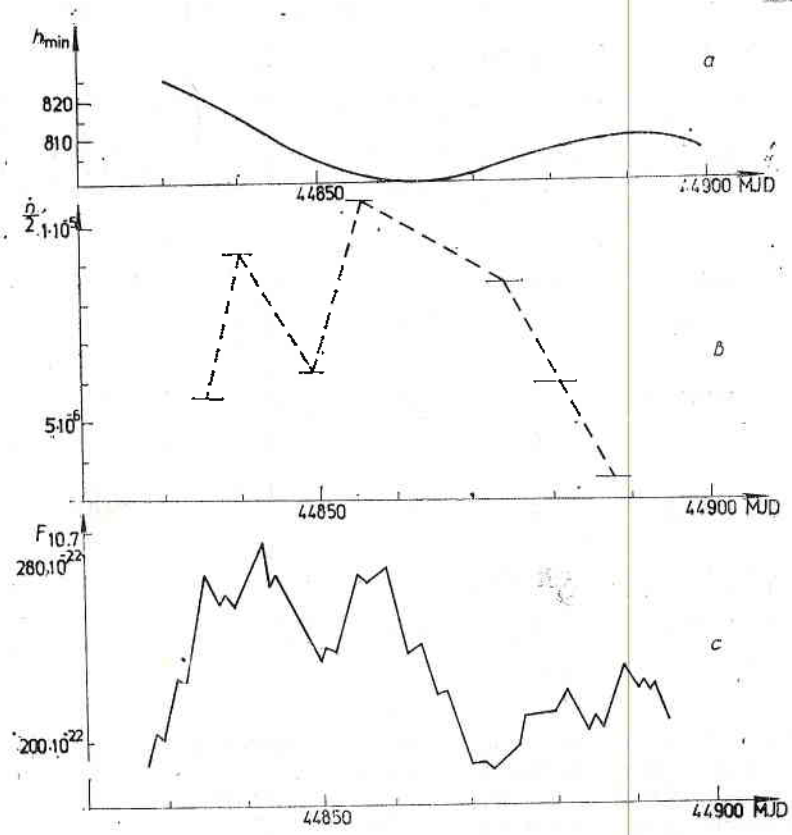

Fig. 1. Graphs of the changes in: a — the minimum height h_{min} (km); b — the atmospheric coefficient $n/2$; and c — the index of solar activity F 10.7, as functions of the time T (in mean Julian days — MJD) for a chosen period of the motion of the artificial Earth's satellite INTERCOSMOS-BULGARIA-1300

values of the atmospheric coefficient $\left(\frac{\dot{n}}{2}\right)$ are presented in Fig. 1, showing the dependence of changes in $\left(\frac{\dot{n}}{2}\right)$ on variations in F 10.7. The change of the satellite height is shown in the upper part of Fig. 1 for the same period of time.

A method of differential improvement of the orbit, using the analytical theory developed by [4], was applied for the calculations of more precise values of the orbital elements of the satellite from laser observations for the same period at the State Astronomical Institute (USSR) [3]. The intermediate orbit is an orbit of the generalized problem of two fixed centres. The algorithm of filtration is the least squares method. The theory of motion takes into account perturbations from the geopotential up to the 20th order harmonics. Lunar

and solar perturbations and secular perturbations are in the atmospheric drag. The model of the geopotential is GEM-10.

Six elements of the intermediate satellite orbit and the coefficient of the secular change of the mean motion were improved parameters. Unlike other analogous programs, the secular changes of the other elements are found from theory.

Eleven series of observations at intervals from 3 to 5 days have been used to study perturbations in the satellite INTERCOSMOS-BULGARIA-1300 motion.

Following conclusion can be made from the results obtained:

1. The theory of the motion for the satellite BULGARIA-1300 gives a satisfactory accuracy at intervals up to 5 days, the mean square discrepances between measured and theoretical ranges being about 3 to 10 m. It is necessary to take more precisely into account perturbations of the atmospheric drag, including variations of atmospheric density with time at intervals longer than 5 days, in order to increase the accuracy of the theory. Theoretically, the accuracy of determination of the angular orbital elements, obtained by the least squares method, is about 0.3 seconds of arc. The actual accuracy, as estimated from two nearby determinations, is 4 seconds of arc. This may be explained by the instability of the atmospheric density, and perturbations that were not taken into account, as well as by the small number of stations that took part in laser observation of the satellite INTERCOSMOS-BULGARIA-1300.

2. The accuracy of laser observations utilized in our work for various passages of the satellite and for various stations varies from 0,8 to 5 m.

3. The obtained laser observations of the satellite INTERCOSMOS-BULGARIA-1300 can be used for studying orbital changes and factors influencing its motion. These observations can be used for positioning by dynamical methods in an accuracy limit 2-5 m. A joint processing of laser and photographic observations of the satellite, obtained at stations Riga, Zvenigorod and Simeiz at a two-day interval in June 1982 in a period of solar activity ($F_{10.7}=160\times10^{-22}$), has been carried out at the Astronomical Council within the ORBITA program [5], founded on the numerical integration of the motion equation. Perturbations of the gravitational field were taken into account only for harmonics up to the order 8. As estimation shows very large errors [6] in the determination of the satellite radius-vector (see below) appear, if changes of the atmospheric density are not taken into account, as compared with calculations based on the atmospheric model DTM 7.

$t=0{,}5$ days $\quad \Delta r=16$ m

$t=1$ day $\quad \Delta r=62$ m

$t=1{,}5$ days $\quad \Delta r=135$ m

The mean square errors of the forecast of the orbital elements on a two-day interval, as computed by the ORBITA program, are:

$m_a=1$ m; $m_e=5.10^{-6}$; $m_i=5°.10^{-4}$; $m_n=4°.10^{-4}$; $m_{\dot{n}}=4°.10^{-2}$.

References

1. Georgiev, N. Bulgarian Artificial Satellite B-1300. — CSTG Bulletin No 3, July, 1981.
2. Хаджийски, А., Н. Георгиев, Вл. Диков. Оптическая лазерная светоотражательная система для спутника ИНТЕРКОСМОС-Болгария-1300. — Научно-экспериментальная программа оптических наблюдений спутника ИКБ-1300, Астрономический Совет АН СССР. Москва, 1984.

3. Эльясберг, П. Е. и др. Обработка данных лазерных наблюдений спутника „Интеркосмос-Болгария-1300". — Бюл. Наблюдения ИСЗ, 1983, 21.
4. Емельянов, Н. В. Определение элементов орбиты „Интеркосмос-Болгария-1300" по лазерным наблюдениям. — Бюл. Наблюдения ИСЗ, 1983, 21.
5. Кужелев, С. В. Исследование численного метода экстраполяции для прогнозирования движения ИСЗ. — Бюл. Наблюдения ИСЗ, 1982, 20, 334—342.
6. Касименко, Т. В., Н. А. Сорокин. Влияние торможения атмосферы на движение спутника „Интеркосмос-Болгария-1300". — Бюл. Наблюдения ИСЗ, 1985, 22.

Геодезический эксперимент со спутником ИНТЕРКОСМОС-БОЛГАРИЯ-1300

Н. И. Георгиев, А. Г. Масевич

(Резюме)

В работе даны первые результаты лазерных наблюдений спутника „Интеркосмос-Болгария-1300". На основе полученных результатов станциями Рига, Симеиз, Звенигород и Потсдам сделаны количественные оценки влияния атмосферы на скорость движения спутника. На основе анализа результатов сделаны выводы о качествах используемых аналитических теорий обработки наблюдений и возможностей спутников с общим предназначением с целью решения вопросов, связанных с определением влияния верхней атмосферы на движение спутников.

BULGARIAN ACADEMY OF SCIENCES

SPACE RESEARCH IN BULGARIA, 5

Sofia . 1986

Mathematical/Statistical Methods for Classification of Objects by Means of Spectral Reflective Characteristics

T. K. Yanev, D. N. Mishev

The resolution of the problems of the earth surface and atmosphere remote sensing relates to the measurement of various quantitative parameters of the electromagnetic field. These are mainly parameters of the solar radiation, reflected from the earth surface and transformed by the atmosphere, as well as of the proper thermal radiation of the earth-atmosphere system.

We have to mention first the spectral reflective signatures (SRS) and in particular the spectral reflective coefficient (SRC).

The SRS is a photometric function representative of the solar radiation structure, dissipated from the various elements of the surface of a given natural formation. The SRS is a multiple function of variables characterizing the physico-chemical and biological properties of the studied natural formations and the conditions required to obtain the SRS (illumination, atmospheric conditions, etc.) That is why the SRS is a multifactorial function containing specific information on the objects it has been obtained from.

I. SRS features

In order to complete a SRS classifier (see point II.), it is reasonable to group the factors that define the SRS values according to some of their general features. Further 'feature' will mean a factor that affects the SRS in a clearly expressed way. The features may be grouped as follows:

A. Primary features — defining the function of reflected solar radiation, trapped at the input of the measurement system;

a) intrinsic features of the studied subject:

— subject-specifying which characterize the elementary unit representative of the subject properties;

— geometric (shape, surface, structure, etc.).

b) external features (atmospheric conditions, illumination, air and soil temperature, soil and air moisture, soil electroconductivity, orientation of the measurement system, etc.).

B. Secondary features which are the SRS values, measured in the individual channels of the multizonal measuring systems.

C. Generalized features obtained in the processing of the primary and secondary features after being treated with certain operator (mathematical, taxonomic, etc.). The generalized features may be grouped into:

a) generalized primary features, for example, type-kind and subkind, forming the taxonomic features within the natural classification of the subjects: soil, vegetation, water, etc.

b) generalized secondary features obtained after mathematical transformations of the SRS.

II. Aim of the SRS analysis

The necessity to study and classify the SRS results from the possibility of their application in agriculture, geology, ecology, etc. The formal expression of the SRS applications in this respect is: to define the relationship between the SRS and the other features (primary and secondary-generalized), in order to resolve the reverse problem; based on the SRS information to reconstruct partially or entirely the values of the primary features (and their generalizations). Such a reversible relation is the classifier. It could be compiled on taxonomic, probabilistic, set-structured, regressive, physical modelling, etc. principle.

IIII. Specific features of SRS

The SRS are random functions obtained in discrete shape (spectrum along the wavelength) under conditions of incomplete apriori information and significant accompanying noise. These specifics require the implementation of statistic-probabilistic techniques for the SRS analysis.

The larger portion of subject-specifying features (including quantitative generalizations) have joint conditional distributions in the multidimensional space of the signatures that, as a matter of fact, are not intercrossing.

Further the conditional distributions will be briefly referred to as distributions only. In this sense such features may be denoted as discrete (Fig. 1), and at the highest level of generalization as qualitative. Some of the subject-spesifying features (and their generalizations) characterize the state of the given subject only (for example, various evolution stages) and may have intercrossing distributions, but of differentiated modes, i. e. they are quazi-discrete. The external features (parameters) may have largely overlapping distributions resulting in smooth transition of the parametric surfaces into the multidimensional space. Such features may be denoted as continuous (quantitative). In the course of development or formation of the subject, for example soils, the transition into a stage (or type or kind) possibly can be performed smoothly, but for the purpose of our Classifier well-shaped states are of interest and this defines the necessity of introducing the quasi-discrete features. Regardless of the eventual smooth transition between them, the probability of distinguishing them is defined with the possibility of identifying various states of the studied subjects in their set of features.

Another important specificity of the features is that they are random magnitudes in terms of our lack of knowledge on their expected values in the progress of the experiment.

a) The primary features (and their generalizations) are random due to inaccuracy of the measuring instruments and insufficient volume of the representative samples in the course of the experiment.

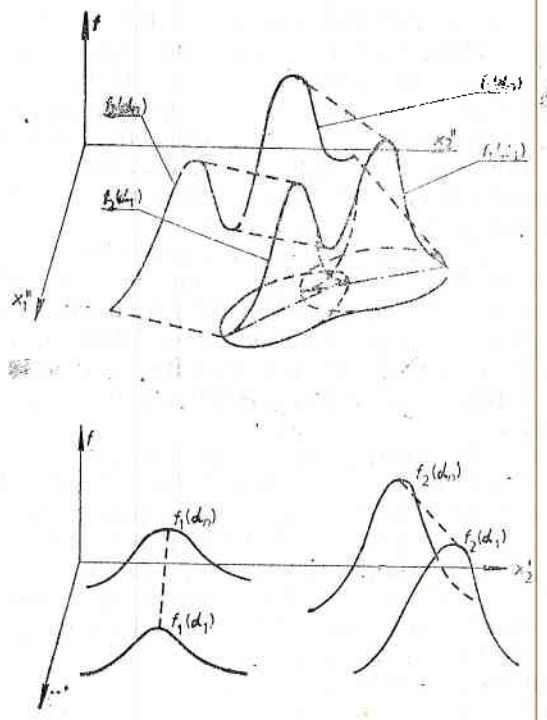

Fig. 1. Discrete and quasi-discrete feature distributions

x_1', x_2' — discrete features;
x_1'', x_2'' — quasi-discrete features;
f — distribution density;
α — parameter

b) The SRS are random functions due both to the reasons innumerated here and in a), as well as to the impossibility to study all primary features affecting the SRS. This problem will be discussed in detail in point IV.

IV. Major problems

As it was already mentioned, the main purpose is to define the relationship between the SRS and the other features. The precise analytical shape of this relationship still seems an irresolvable problem. The various stages of approximation to this task could be formulated as follows:

Physical model of SRS.

At the available state of our knowledge this is possible only for some particular relations between the SRS and the primary features. The modest results attained by now do not permit large-scale applications in agriculture.

Statistical Model of SRS.

This is realized with the determination of the regressive dependence (surface in the multidimensional space of the feature) between SRS and a given set of primary features or their generalizations. There is no available method by now to define the confidence regions of such a regression in the general case, when both the features and the dependence value (the SRS in this case) are random variables [1]. The Classifier procedure requires to know these confidence regions. Relatively easier is the problem of regression coefficients determination. This can be done using, for example, the method of the maximum likelihood [1], the method of least squares [2], etc., and the regression is traced between the i-th component of the SRS $\mathbf{r}$ vector and all the k-th components of the $\boldsymbol{\alpha}$ vector of the features, $k=1, \ldots, K$

$r_i=f(\alpha_1, \ldots, \alpha_k)$, $i=1, \ldots, m$-channel number for SRS.

The confidence intervals of the regression may be defined with certain inaccuracy with the available techniques (which require for the independent variables of the regression to be determined variables) if we can ensure that the relative variance (measured for example, with the variation coefficients) of the primary features (and their generalizations) is at least of an order smaller than that of the SRS.

The evaluation in this respect may be obtained, if we compare the vector of the relative errors δ_α of the vector $\boldsymbol{\alpha}$ of the primary features (including their generalizations) and the vector of the relative errors δ_r of the vector $\mathbf{r}(\boldsymbol{\lambda}, \boldsymbol{\alpha})$ of the secondary features (incl. their generalizations). If δ is assumed to be measured with the variation coefficient, then $\delta_l=S_l/\mu_l$, where μ_l is the average value of the l-th component of $\mathbf{r}$, respectively $\boldsymbol{\alpha}$, and S_l is an estimate of its mean square deviations. Basic sources for δ_α and δ_r formation are respectively (p. A for δ_α and p. B for δ_r):

A. a) Test field measurements:

i. Errors from the measuring systems.

ii. Errors from the interpolation and extrapolation of the measured data, when studied areas are large and with various conditions (and they must be such in order to receive statistical representation of the data), therefore measurements of sufficient coverage cannot be performed.

b) Remote sensing (helicopters, airplanes, balloons, satellites):

i. Errors from the measurement systems.

ii. Errors from interpolation and extrapolation of the measured values (as for p. A. b).

B. a) Test field measurements:

i. Errors from measurement systems.

ii. Errors from insufficient knowledge on SRS yielding conditions (mainly in evaluating the illumination conditions).

iii. Undetermination of $\mathbf{r}$ in the result of the fact that not all the intrinsic and external features are included in $\boldsymbol{\alpha}$.

b) Remote sensing:

i. Errors from inaccurate evaluation of the SRS yielding conditions (illumination, atmospheric state, etc.).

ii. As in B, a, iii.

All the features incorporated in $\boldsymbol{\alpha}$ (if properly selected) are independent from $\mathbf{r}$ (but they also might be interdependent) and affect the $\mathbf{r}$ values on the cause-effect scheme.

Present experience shows that the $\boldsymbol{\alpha}$ and $\mathbf{r}$ component distributions are close to normal. From the definitions in A and B and the experience acquired, the following conclusions can be made:

C. δ_{Ba1} and δ_{Ba2} are commensurable respectively with δ_{Aa1} and δ_{Bb1}, and δ_{Bb2} is commensurable respectively with δ_{Ab1}.

D. δ_{Ba3} and δ_{Bb3} are commensurable respectively with δ_{Aa2} and δ_{Ab2}.

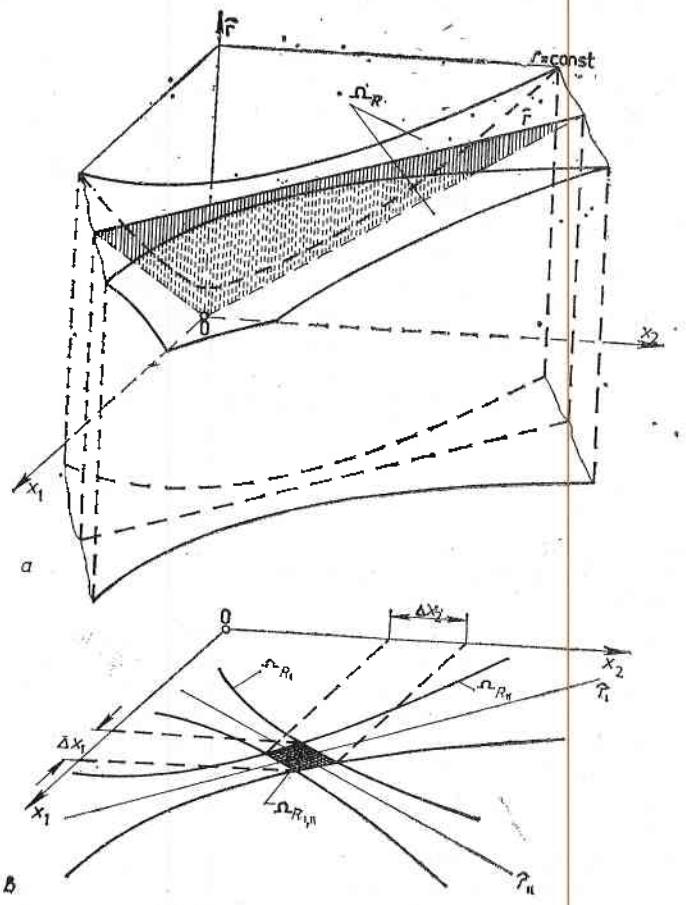

Fig. 2. Confidence regions of regression surfaces

a — three-dimensional regression surface $\hat{r}$ and its confidence region Ω_R;

b — two-dimensional projects of confidence regions Ω_{R_I} and $\Omega_{R_{II}}$ and their cross section $\Omega_{R_{I,II}}$

The errors from D are much larger than from C. The available experimental possibilities provide for a significant reduction of δ_{Aa2} only as compared to the other δ from D. Therefore, a regression with confidence intervals determination can be effectively traced (at least at present) only between r and α on test field data, if a sufficient number of well planned experiments is available with δ_{A2} is at least an order smaller than δ_{Ba3}.

The possibility to obtain regression with a confidence region still does not lead to an easy practical application, at least due to:

1. The confidence regions Ω_R (Fig. 2) are defined for the regression surface parameters and the classifier requires the confidence region of the individual result $\Omega_I \approx \Omega_R \cap \Omega_{IS}$ to be known, where Ω_{IS} is the sample value of Ω_I.

2. The determination of Ω_R and Ω_{IS} is related to significant computation difficulties. Fig. 2 shows the case of two dimensional regressions (α contains two features). Even in this relatively simplified case the analytic (and respectively the automatic) determination of Ω_R is significantly hampered. We should add to the necessity of plotting the Ω_R projections over the coordinate system axes the necessity of knowing the confidence intervals of the individual parameters (features). Additional difficulties result from the determination of Ω_{IS}. Certain facilitation may be achieved if r is obtained as a mean square from the multiple resolution elements (RE), each of a dimension representative of the least possible RE, already marked with the properties of the studied class. Then Ω_{IS} will tend to Ω_R. This case reveals the problem of determining the minimum RE dimensions. Anyway, such a problem should be resolved in general prior to the large-scale SRS measurements, in order to determine for each class or theme of classes (although approximately) the optimal RE dimension in agreement with beforehand selected criteria. In [3] there is a solution through which the optimal RE dimension is defined in the course of the experiment. Certain general methods and instrumental requirements for site-testing in the ground-based studies of SRS are given in [4,5].

Another problem related to RE of SRS is the case when mixture of two or more thematic classes is available in RE (i. e. such that will be of interest to the interpreter) and a separation of this mixture is required. In general, the separation of SRS mixture is a problem of two main aspects:

— separation of a mixture from SRS distributions obtained from a RE set (pixel), within the limits of which RE there is no mixture of SRS of different classes, and

— separation of SRS mixture, obtained within the limits of one RE.

The first problem is closely related to the selection of optimal RS dimension. Under proper selection, if possible, i. e. if a plateau exists within the limits of the studied region, the problem does not exist at the interpretation level. In the reversible case the SRS distribution from various RE is obtained in polymode. Under defined conditions, for example, identification of the distribution type, the component number determination is performed with the well known methods [6].

The second problem requires solution when two or more interpetation classes are mixed within the RE limits [7,10] and their percentage participation is sought (weight coefficient) in their collective SRS. Such case is represented, for example, with series of agricultural crops divided by soil strips. The problem is solvable in the statistical sense, if the class distribution number is known for the classes participating in the mixture and their parameters. Then the confidence intervals can be defined for the weight coefficients when sufficient channel number in the SRS measuring system is available.

In conclusion we may say that the elaboration of general regressive function $r(\lambda, \alpha)$ is still very difficult both on methodological and applicable computing level. Therefore, in near future it is possible to obtain only particular regressive dependences of largely limited α dimensionality. Nevertheless, we consider that even so the information will be useful for the SRS interpretation.

Probabilistic-set classifier

This classifier is built by comparing the confidence regions of the primary features and their generalizations with the confidence regions of the SRS or their transformations. The adequacy of this comparison with the available apriori information, as well as the updating with the experience acquired is controlled by

the interpreter. This approach is suitable for the discrete and quasi-discrete features mainly. The major stages in the compilation and operation of such a classifier are:

a) training — with and without supervisor,
b) classification and new information accumulation,
c) updating,
d) dimensionality reduction of the features space in a given thematic class set.

Further, a largely simplified scheme of the SRS classifier is applied. This is compiled within the attempt to balance the two basic contradictory requirements: application simplicity and sufficient accuracy of the classificaton.

The following exposure contains in brief and in a time-generalized form the fundamental information for the structural units of the suggested scheme and also a brief comparative analysis of some available methods and approaches related to the discussed problem.

V. SRS Classifier

1. SRS Transformations

The basic criterion of effectiveness for a given transformation is the risk function R (Appendix 1). In a fixed set of classes the transformation which reduces R to a higher degree should be adapted as more efficient. The evaluation of R in most of the cases is difficult. Some indirect criteria are known that are used as alternatives in first approximation of R linear and nonlinear functions of the intra- and interset class distances (clusters respectively), enthropic criteria, etc. In the case when the class distributions are close to normal we assume as the clearest and in many cases directly proportional the relationship between the variation coefficient V of $\vec{r}$ (by components) and $R: V_i = \sigma_{r_i}/r_i$, $i=1, \ldots, m$ — channel number of SRS. Further on, when possible, it will be preferred as a measure of effectiveness for the transformation replacing R. The main types of transformations that are available are:

1.1. Orthogonal (expanded by orthogonal functions).

a) non-eigen systems of orthogonal functions: Fourier, Walsh, Hadamard, Vilenkin-Chrestenson, orthogonal polynomials, etc. No direct data are available as to whether the use of these expansions coefficients as $\vec{r}$ components in the transformed space results in V reduction. It may be demonstrated in particular that for the Fourier transformations such a reduction is not guaranteed (see Appendix 2).

Another defect of these transformations is that when steep SRS sectors are available (for example, vegetation), a large number of expansion components is necessary which increases the dimension of the transformed space. Also these transformations assume that SRS are periodic functions, i. e. a compromise with reality which results in description inaccuracy.

b) eigen systems — transformations of Karhunen-Loeve (in the discrete version a method of the main components). The advantage of these transformations is that no SRS periodicity is required here. The disadvantage being that the eigen systems of the j-th class is optimal with respect to the economic class description only for this class, and not for the other classes from the classifier set examined. That is why, the switch-off of some SRS channels after the analysis of the given class in its eigen system may negatively affect

R within a given situation of the class description in the set (for example, it is possible to identify well some of the classes precisely in these channels).

1.2. Autocorrelative transformations (some formulae are given in Appendix 3).

The advantages of these transformations are: dimension of the transformed space not larger than that of the primary space; the variation coefficient of r in the transformed space is smaller than that of the primary space; simple calculation operations for transformation. As a disadvantage we may point out the ambiguity of the transformations II and IV in the sense that equal autocorrelative functions may be derived from various functions. But this ambiguity includes a class of symmetrical functions to the coordinate axes, and such symmetries cannot be found in SRS of the natural formations over the Earth surface.

1.3. Enthropic transformations (Appendix 4).

As it is already known, they are realized in eigen coordinate systems [9, 13], and, therefore, the summary of p. 1.1. refers to them also.

1.4. Divergency transformations (Appendix 4).

They lead to the optimal results in the sense of minimizing the defined divergency only for a given couple of classes and, therefore, the disadvantage of the eigen transformations from p. 1.1. In addition, they involve a very large number of calculations, and information losses in the real case in unequal covariant matrix of the classes [9].

1.5. Metric measures for similarity and distance optimization bewteen vectors-realizations.

According to the type of the distance metrics, these transformations divide into: (A) Euclidian; (B) Mahalanobissian, etc.; and by the optimization criterion into: (a) minimizing intraset distances; (b) maximizing interset distances, and (c) mixed.

i. Complex (in the sense of a certain criterial function) distance optimization [9, 11, 12, 13] and ii. Serial realization of a) and b). Usually (A) methods are based on linear transformations and relate directy to (a) and (b). (A, a) transformations lead also to enthropic transformations. The non-parametric Patrick-Fisher transformations [13] use the exponential function as a criterion that increases with the expansion of the interset distance and the reverse, and relates to (c).

The advantages of these transformations are mainly two: they have a completed analytical technique for determination of the transformation matrix, and provide possibility to improve the class separation in the sense of the defined criteria, but without a direct link with R.

The disadvantages are grouped into: i. criteria (a) do not guarantee separately the obligatory decrease of R; ii. criteria (c) make it possible to evaluate in explicit form the increase of the class separability only when there are two classes, while in the general case of many classes (especially when the primary space is populated with a large density, it is difficult to evaluate beforehand the effect of the global distance change between the realizations. Description of other metric and non-metric clusters-algorithms is given in [9, 11]. The possibility for their application in SRS classification is probably smaller than of the techniques discussed here.

This brief comparative analysis provides certain advantages of the autocorrelative transformations, because it is possible to obtain with them universal (for the complete class set studied) improvement of the class separability, measured in the first approximation with the variation coefficient V and estimated by now for the primary space only, and not for the other types of transformations (These transformations also relate to simple computing operations)

As a general disadvantage of all the mentioned transformations, we shall note the absence of a clear analytical link in the general case of unequal covariance matrices of classes between the risk function in the primary and transformed space. Due to this the transformation effectiveness can be evaluated only approximately in an analytic mode. After the transformation, direct calculations of R must be performed for each beforehand given class set with a theme compiled in the Classifier.

2. Transformations to avoid ill-conditioned covariation matrix

When the channel number of the system for the SRS yield is large, for example 32, there is a possibility for the determinant of the covariation matrix of certain classes either to become smaller than the computer zero (in the case when the SRS are reduced to spectral illumination coefficients smaller than a unit, and therefore, with dispersions of the 10^{-1} order), or to exceed the upper computer limit (for example, when the quantization level number of r_i is of the order of 100-200). A possibility to avoid this ill conditioning due to scale effect is provided, if the primary SRS data are this multiplied with a suitable and equal for all SRS number or through the division of each SRS to its mean arithmetic: this means a reduction to a relative coordinate system and loss of information for the mean class vector, except if it is not introduced as an additional feature. The transformations discussed are not effective when the determinant is ill-conditioned in structure.

3. Subtraction of submatrix

A possibility of reducing the input matrix from dimensions $(m \times n)$ to dimension $(m' \times n)$ is foreseen when it is possible to decrease dimensionality of the primary space of the features.

4. Cluster analysis

It is applied for grouping the input data by some formal criterion of similarity. The quantitative expression of this criterion is the measure of similarity. Usually it is selected as 'distance' in space apriori selected metrics (for example, Euclidian). The following procedures divide the cluster-algorithms into two groups: (a) subjecting the measure of similarity to threshold values through the realization of non-equalities, and (b) optimizing the selected function of this measure, in order to define a criterion (most often for this purpose the transformations from 1.5. are applied). There are tens of well-known cluster-algorithms (nearest neighbouring maximum distance, ISODATA, etc.) [9, 12, 13]. The computations of inter- and intraset distances is performed mainly for algorithms from (b). These operations make difficult the algorithmic application when the number of vector-observations that are subject to clustering is larger than 10^3 [12]. Since in the real case of remote sensing data (and even test field data) for the SRS their number will be larger than 10^3, it is recommendable to fix on the application of more simplified cluster-algorithms) mainly those from (a).

5. Automatic controls

5.1. For cluster population: if population is less than the critical (given by the user) the cluster is not analysed and is entered into the memory.

5.2. For normal cluster distribution: in satisfying the requirements of a given criterion of normality the vector-observations forming the cluster are passed for the calculation of an average vector and covariation matrix.

5.3. For ill-conditioned covariation matrix.

6. Normal distribution simulation

Based on average vectors given by the user, a set of normally distributed vectors is obtained, i. e. classes of normally distributed vectors are modelled. Such data file is necessary for the comparative study of the effectiveness of various transformations or other programs when the real data available are insufficient.

7. Compilation of classifier

7.1. All clusters satisfying the controls (incl. the operator control of clustering accuracy – see explication in 7.5) and all classes formed by the user at the input of the main program are passed for computation of average vector and covariation matrix. Afterwards the information is storaged in the Classifier. The storage may have various variants in dependence on what type of transformation has been applied for its compilation.

7.2. Storage classes limits: (a) with Bayes approach—the limits depend on the set of classes which at a given stage of classifier compilation are compared in determining the risk function. This approach ensures minimum risk function; (b) in beforehand limitation of classes.

i. Multidimensional confidential parallelepipeds with axes parallel to the coordinate axes and multidimensional confidence ellipsoides whose axes have been obtained with sufficient statistic material for the classes (after a training procedure); in this approach the computing operations are largely facilitated, but the value obtained of the risk function is not minimum. Anyway, solution may be looked for at apriori given admissible upper limit of R.

ii. With linear and non-linear decision functions; in this case — the region of a given class is localized with limitations of some of the multidimensional planes and non-linear surfaces. This approach is related to the following significant disadvantages:

— even when the discriminators are linear at a class number larger than 20-30, the oblique multidimensional linear surfaces are complex and result in an inadmissibly large number of computations; in the case of SRS classification, the class and subclass number subject to identification should hardly be smaller than several tens;

— probabilistic evaluation is difficult for the classification quality, moreover that the larger part of these algorithms do not permit probabilistic evaluation and become cycling when the classes intercross (an exception is the algorithm of Ho-Kashyap [9]); iii. In the statistic algorithms for obtaining a decision functions: stochastic approximation, perception approach, potential functions, etc. In this case the convergence of the algorithms to the Bayes classifier is very slow [9]. This disadvantage will be manifested particularly strongly in the SRS classification when the dimension of the feature space and the class number are of the order of several tens and this is the real situation.

Due to the disadvantages demonstrated, the further procedure will consider the limits defined in (a, b. i).

7.3. Risk function computations. Case 7.2.a is computed when apriori information is available on the class distribution, their apriori probabilities and

the loss matrix. Advantages: minimum R_{Bayes} is guaranteed. Disadvantages: usually the apriori information is not available, assumptions in simplified version are needed to be adapted and to be updated in the process of Classifier compilation. Anyhow, when the form of distribution can be assumed with sufficent certainty (in this case the experience acquired in SRS is encouraging [14, 15, 16]) and there is a possibility to increase the representative sample to the volume required, the Bayes approach is recommended [17].

Case 7.2.b has the following advantages as compared with 7.2.a: R constant limits simplified computation; and disadvantages: R value obtained is not minimum at the expense of the cutoff 'tails' of the distributions in the formulation of the class constant limits. The upper limit of $R_{const.\ limit}$ may be calculated with the 'tails.'

7.4. Classification of newly added vector-observations. The referring of the newly added observations to a certain class in the Classifier storage (to none in particular) is defined with the verification of the non-equality system: in the case 7.2 as obtained with the principle of maximum likelyhood, and in the case 7.2.b, i — from the class limits.

7.5. Classifier learning. In the scheme suggested the learning phase is realized as follows:

Unsupervized learning: through the cluster programs in agreement with the introduced formal criterion in them for similarity between observations.

Supervised learning: (a) at the output of the cluster program where in interactive mode the operator controls the clustering quality and corrects the erroneously grouped observations, based on the available apriori information; (b) At the input of the major program: through apriori classified observation files, for example, from test field measurements; c) updating of the Classifier storage. The verification of the normal conditions guaranteed the necessary closeness of class distributions to the normal in the classifier [17] and, therefore, guarantees the Bayes mode of learning of the average vector at sample volume tending to infinity.

The supervised learning is performed with apriori information, and comparison between the confidence SRS regions (and their transformations) with those of the generalized features.

8. Reduction of the feature space dimension

In many cases the identification of a given set of classes can be performed with a beforehand given identification quality (for example, through the permissible maximum R value), with a portion of the information obtained in the experiment (for example, with the SRS values of some channels only). The resolution of this problem results in both direct economy of computations and in optimization of the technical problem with regard to the measurement systems and their exploitation capacity. The result from the resolution of such a problem may serve as a criterion for the effectiveness of certain SRS transformations. Some Basic methods for the reduction of dimensionality of feature space are given in [9].

The precise resolution requires a study of the complete combinatorics of subsurfaces formed with the subset of features (primary and generalized) and a definition of those combinations that satisfy the selected criterion of the classification quality. In the general case of unequal covariation matrices and non-linear decision functions this problem is difficult to be realized in regard to the computation efforts involved. But if we assume that the covariation matrices, though unequal, are diagonal (of diagonals equal to

those of the real matrices) and the classes are limited with multidimensional parallelepipeds, including the confidence ellipsoids whose axes are parallel to the coordinates due to the diagonality of their covariation matrices, then the problem reduces to a problem of technical diagnostics. A possible solution is suggested in [18], where the V value is the criterion for the classification quality. In the scheme thus suggested the problem is resolved with the combinatorics program. The restrictions introduced in the resolution of the problem in this case result in the following: if the program provides an answer that given subset of features is sufficient for the classification of the studied set of classes, then this conclusion is preserved in the general case also for the nondiagonal covariation matrices, but the risk function in the general case will be smaller. The reverse answer that the given feature subset is not sufficient for the set class recognition at a fixed value, is not a guarantee that at nondiagonal matrices the same result will be preserved.

9. Coupling of classified realizations with geographic coordinates and contouring of the spectral homogeneous regions

In order to resolve this problem, it is necessary to provide accompanying code for each vector-observation through which the geographic coordinates of RE can be compared. With the help of plotter-programs in a two-dimensional coordinate system, the coordinates of all the observations of a given class are plotted. When simultaneous visualizations are needed (graphs) of more than one class, several well distinguished symbols are used. The computation of the geometric characteristics of the contoured regions can be provided with upplementary programs: perimeter, surface, formfactor, etc.

10. Classifier storage updating

All classified and unclassified realizations entered in the Classifier are memorized according to the type of the classification programs (Bayes, multidimensional ellipsoid, etc.), and the type of the apriori SRS transformations.

After accumulating a given quantity of such data the updating is performed (on user's request) in two directions:

A. With the already classified observations the average vector and the covariation matrix of each available class in the storage is updated. It is advisable for the purpose to use numerical models for brief computations [9]. This approach assumes the implementation of nonmarked training sequences of SRS in the classification of new observations, i. e. for which it is not apriori known to which class they belong. Therefore, if in the classification mode at the input of the program the maked training sequence is fed, the information from the unclassified observations cannot be used for direct updating of resolution surface parameters. This may be performed, if the techniques of stochastic approximation are applied for the iterative determination of these parameters.

B. With the unclassified realizations to any classes in the storage and also with those that have not satisfied the automatic controls. For the purpose, an input file is composed from them and the complete training cycle is performed with it. Here it is possible to produce new classes.

In the process of compiling a thematic classifier of finite number M_{max} of forming classes it is possible to obtain as an intermediate result $R_{Bayes} < R_{const.\ limits}$ when the nonequality $M < M_{max}$ exists. This is due to the following: Bayes SRS classifier operates with theoretical normal distributions that are de-

fined in the interval $(-\infty, \infty)$ for each of the features. After the first learning stage (no updating was made) the class number is $M<M_{max}$ (in the real case at the recent stage of knowledge on SRS not always the apriori precise classifier content may be available even for relatively limited themes). On the other hand, in the next stage, classification, again for the real case of space and airborne data processing observations that may belong to $M+j$-th classes, $j=M+1, \ldots, M_{max}$ may be entered. If $M \ll M_{max}$, the distance between the centers of M-th classes is relatively large with regard to the available filling of the thematic feature space. Due to this and also to continuity of the normal distributions in the intervals $(-\infty, \infty)$, the Bayes decision functions limiting the available classes pass away from the class centers. Thus probability increases for observations belonging to the $M+j$-th class to be classified as belonging to some of the M-th classes if $M+j$-th class is close to some of the M-th classes. Such an error of II gender can be reduced, if the performed M classes are limited with, for example, confidence ellipsoids or parallelepipeds of smaller size and not with Bayes functions, but anyhow such that the sum of the cutoff tails of the normal distributions would be admissible, i. e. the error of I gender would not exceed the apriori limit. Then the possibility for realization from the $M+j$-th class to enter some of the M-th classes is considerably reduced, except for if in general the $M+j$-th class does not intercross largely with some of the M-th classes. After repeated updating the classifier will be refilled with new classes and when $M \to M_{max}$ then $R_{Bayes} \sim R_{const}$ will be ensured. Therefore, when the updating is performed: a) under condition $M < M_{max}$; b) with data of no apriori information as to whether they belong to the M-th formed class only, it is recommendable to complete the classifier, using confidence ellipsoids or parallelepipeds and only under $M \to M_{max}$ (the criterion for this may be the absence of new class formation after repeated updating within the theme) to apply the Bayes decision functions.

For the given confidence decision functions it is possible at fixed value M (by number and class content) to minimize the risk function [19]. Of course, the minimum R_{min} thus obtained will be larger than R_{Bayes}, if realizations belonging to the M-th class are entered only.

VI. Program package for classification of spectral reflectance signatures

When determining the structure and the content of a program package designed for the classification of spectral reflectance signatures (SRS), multiple considerations from both general and particular nature must be taken into account in view of the package effectiveness: scientific, economic and applicable. Some of these considerations were discussed in the previous chapters. Considerations, related to the experimental specifics of SRS obtaining and affecting the volume of the computation efforts under application of program package for SRS classification, may be generalized as follows:

1. In the real case of satellite and nonsatellite information use for classification or for learning files, thousand or tens of thousand SRS are applied (vector-realizations in multidimensional signature space) as obtained from individual elements of solution.

2. Class and subclass number that is interpreted within the limits of the thematical classifiers, for example, for agricultural purposes, is of the order of several tens.

3. The dimension of the primary feature space (the channel number of the multispectral devices) in which SRS are obtained is also several tens for the contemporary technical provisions.

4. The SRS distribution is in most of the cases sufficiently close to the normal, due to which there are grounds to apply the respective statistical methods elaborated for normal distributions.

The major operational modes for the SRS Classifier usually are: training, classification and updating. According to the selected algorithms for determination of the class characteristics, these three modes may be realized both parallel or in sequence, for example, the techniques of the stochastic approximation require parallel performance of training and updating to achieve more complete information use for the incrorrectly classified marked realizations in the training sample, but this involves larger computation efforts, that must be taken into account due to the considerations in 1, 2 and 3.

It follows from the considerations 1, 2 and 3 that the necessity of decrease in the dimension of the feature space, where the SRS classification or one of their transformations is performed, should be also considered. This can be realized through appropriate SRS transformations and determination of the minimal feature combination (under beforehand given class set) and thus to attain the given threshold value of the risk function or of another criterion on the classification quality [9]. In the general case when the covariation matrices of the classes are not equal, the relationship between the risk function R and the various criteria for classification quality is established rather nonreliably after reduction of the feature space.

Consideration 1 should be taken into account when selecting the cluster-algorithms with preference to those where the training matrix is used in series, column by column, with no necessity to be kept entirely in the operational memory, as is the case with the cluster-algorithms that optimize the criterion functions from intra- or intergroup distances, etc. In cases similar to the latter, the acceptable dimension of the training matrix is no more than 1000-2000 vector-realizations.

Consideration 4 makes possible the use of probabilistic methods for classification that are more precise than the cluster-algorithms or the determined discriminant functions (hiperplanar, etc.) and provide possibility to compute or evaluate the function of the average risk.

Accelerated computing procedures are applied to obtain separate mathematical functions as the probabilistic integral in the multidimensional feature space, the average vector and the covariational matrix of each class and the algorithms for their updating, etc. In [27] an accelerated procedure is suggested for classification by Bayes through replacement of some of Bayes decision functions in the course of the procedure with simpler criterion nonequalities, and also through appropriate transformations of the covariation matrix.

Significant alleviation of the computation efforts may be obtained through the application of the confidence hiperparallelepipeds as a prefilter to Bayes procedure of classification. In this case, the verification of the belonging of vector $\mathbf{X}$ to a given class is initiated with a system of nonequations

$$a_{ij} \leq X_i \leq b_{ij}, \quad i=1, \ldots, m, \quad j=1, \ldots, n, \tag{1}$$

where m is the dimension of x, n is the number of classes in the Classifier, and a_{ij} and b_{ij} are the limits of the hiperparallelepiped of the j-th class. These limits may be determined differently, for example, so that the respective confidence ellipsoid should be inscribed in it (determined at a given confidence level) or so that the shaping edges of the parallelepiped would equal the res-

pective main axes of the ellipsoid (then the latter will be incorporated into the hiperparallelepiped) and so on. In agreement with consideration 4, the dimensions of the ellipsoid can be determined on the basis of the normal distribution. If under a fixed j at least one of the non-equations (1) is not fulfilled, then the vector $\mathbf{x}$ does not belong to the j-th class (under selected confidence level). In the reverse case the answer that $\mathbf{x}$ belongs to the j-th class is not absolutely positive, because it is possible that the j-th hiperparallelepiped would have section $\Omega_{jk} \neq 0$ with another k-th hiperparallelepiped. Under a built thematical classifier the indices k of the classes for which $\Omega_{jk} \neq 0$ should be kept in its memory for a given j and also when it is established that the system (1) under fixed j is satisfied by $\mathbf{x}$, Bayes classification should be performed for those values of k only for which $\Omega_{jk} \neq 0$. Similarly, the classification with the help of hiperellipsoid may be performed. System (1) requires simple computation operations without necessity to compute the Mahalanobissian distance in a prestage and, therefore, we may expect significant fast action of the procedure described. It is possible when we have significant amount of closely located classes in the Classifier to perform a combination of the upper procedure with the one sugested in [27] at the second stage (when it is established that $\mathbf{x}$ satisfies (1) and $\Omega_{jk} \neq 0$ for several values of k) that will result in a greater acceleration of the classifying procedure, especially in the case when the covariational matrices of the classes have eigen numbers that differ in-between.

An example of the structure of a program package for SRS classification, taking into account the above-mentioned considerations, is shown in Fig. 3. The denomination of the subprograms and their destination are as follows:

1 — input matrix of data; *2* — multiplication of the input matrix with constant number; *3* — cluster-algorithms; *4* — SRS transformations; *5* — multiplication of vector-column by normal law; *6* — verification of normality of the cluster-formed distributions; *7* — determination of a mean vector and covariation matrix of the normally distributed sets of SRS vectors or of their transformations; (7_1 — through initial training file, 7_2 — through the method of stochastic approximation, 7_3 — through updating with accumulated data for correctly classified vector-realizations); *8* — control of ill-determined covariation matrix; *9* — computation of the risk function by Bayes; *10* — computation of the risk function under decision surfaces, composed with hiperparallelepipeds and hiperellipsoids; *11* — classification by Bayes; *12* — classification with hiperparallelepipeds and hiperellipsoids decision surfaces; *13* — subprogram for dimension decrease of the feature space; *14* — subprogram for yielding in *X-Y* spatial coordinate system (plotter) of the vector-realizations, classified to one class (spectrally homogenious regions).

File β contains the mean vectors μ and the covariation matrices K of the formed classes as follows: β_1 — without pretransformation on the input matrix; β_2 — after transformation of the input matrix with some of the transformations in subprogram *4*; β_3 — after fulfilment of subprograms *5*; β_4 — after fulfilment of subprograms *4* and *5*; β_5 — through training matrix in which the classes are formed by blocks.

File α contains the vector-realizations for updating.

In α_1 the information from following groups is stored:

a) clusters, where the quantity of realizations is smaller than a critical number pregiven by the user, the value of which is determined from the type of the criterion of normality in subprogram *6*;

b) clusters that have not satisfied the requirements for normality in *6*;

c) clusters or sets of vector-realizations, determined as classes of subprogram *5*, or through the training matrix, determined for file β. These clusters or sets have ill-determined covariation matrix.

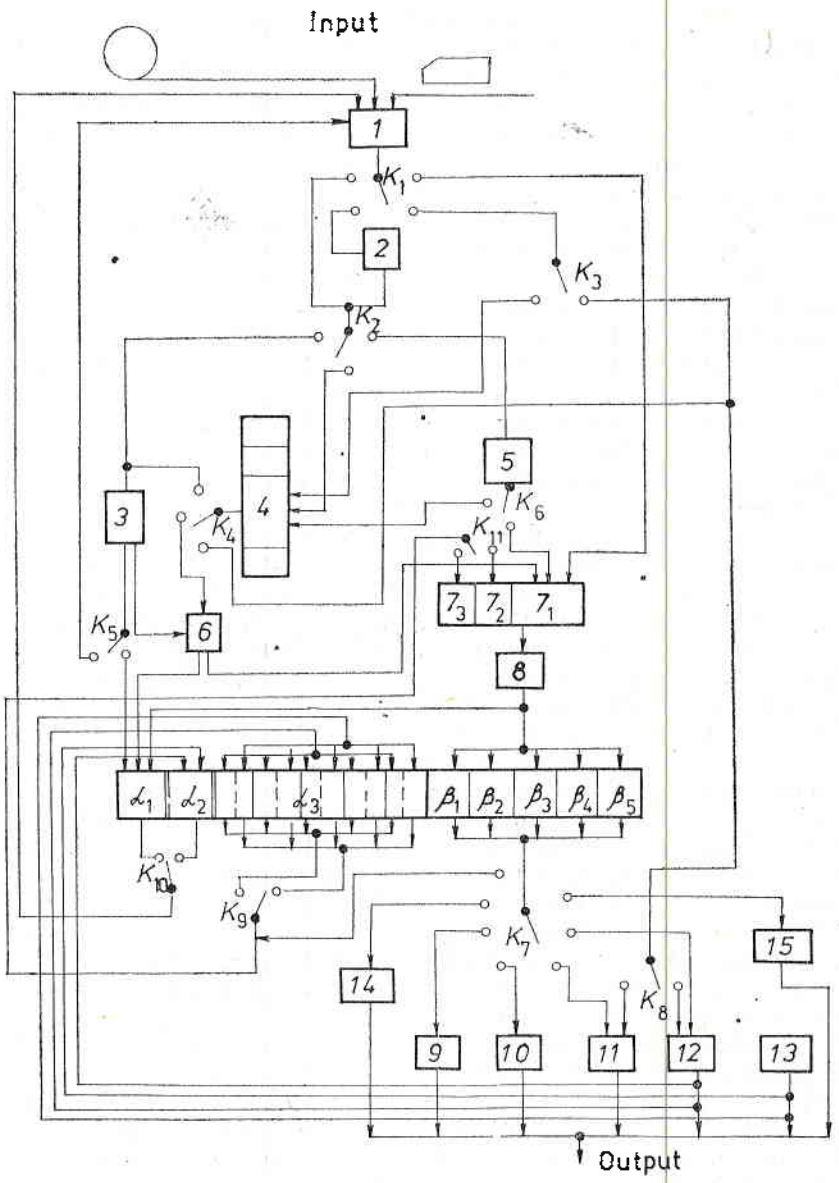

Fig. 3. An example of structure of program package for a spectral reflective signatures (SRS) classifier

Information on the vector-realizations that is not classified to any of the classes in file β is stored in α_2.

File α_3 contains vector-realizations classified to some of the classes in file β (information of the field number of file β together with information by which

subprogram the classification was performed: 11, respectively 12, is stored and this information is used in the updating).

Through the various states of variables $K_1, \ldots, K_{11}$, the mode of package operation is determined on the user's request.

Principal modes of operation of the package are:

Training.

a) With teacher: this is realized with marked training input matrices and the final result is the formation of the classes in β_1, β_2, β_5 and the computation of the risk function for the set of classes obtained;

b) Without teacher: this is realized through unmarked input matrices (the real case suggests operational conditions of incomplete apriori information) that pass through subprogram *3* (possibly in combination with *4*); through the variable K_5 the operator may verify the correctness of the clustering, based on the apriori information available, and then to exclude the incorrectly introduced vector-realization in a given cluster from the input matrix and to start again the selected sequence of subprograms with the new matrix thus formed; the final result is the formation of the classes in β_1 and β_2;

c) For research purposes files β_3 and β_4 are used in which model classes are formed through subprograms *5*, respectively *5* and *4*, in order to verify the possibilities of the various types of transformations, both with respect to the size of the risk function and to the decrease in the dimension of the feature space (for the purpose subprogram *15* is used).

Classification.

This mode of operation performs the classification of the unmarked vector-realizations through subprograms *11*, respectively *12*. If the classification is performed in field β_2, the vector-realizations are beforehand transformed with the transformation from *4* through which the classes in β_2 have been obtained. Finally decisions for the belonging of the vector-realizations are obtained in print, and the vectors are sent to α_1, respectively to α_2, for updating of the classes characteristics (using the stochastic approximation, the updating can be performed in the real time mode).

Updating.

The updating of the classes characteristics (mean vector and covariation matrix) from file β is performed in two modes:

a) through formation of an input matrix from data in α_1, α_2 or mixture of the two files after which operation is performed as in the 'training' mode;

b) from file α_3 in 7_b, respectively 7_c, the vector-realizations are introduced considering the field of file β that is updated. File α_3 contains the fields, corresponding to those of β and additional subfields in respect to which subprogram *11* or *12* was used to perform the classification. These are shown with dotted-line in Fig. 3.

The first version of the above-described program package is realized in the Central Laboratory for Space Research at the Bulgarian Academy of Sciences on FORTRAN IV and ASSEMBLER languages and under the control of OC/EC.

Chapters I to IV are composed based on works [25] and [28] and chapter V is based on work [26].

Conclusion

The approaches examined (major tasks) are of downward sequence of complexity, resulting from available possibilities: physical models, regression models, probabilistic-set classifier. Undoubtedly, the physical models are the most de-

sirable result for the experimenter and the interpreter, but they are resolvable in long-term perspective. The general regressive models are irresolvable in practice by now, although partial solution is acceptable in principle with the limitations as given above. The closest relative perspective for direct practical applications on a larger agricultural scale is that of the third approach, although the absence of sufficient apriori information and the disturbing atmospheric effect and other noise sources reduce its effectiveness.

Appendix 1

Risk function [9, 12]

Each SRS is represented as m-dimensional vector $\mathbf{r}:\{\mathbf{r}_i\}$, $i=1, \ldots, m$-SRS channel number. The compatible by a given criterion of similarity vectors $\mathbf{r}_{jk}$ form the k-th class of population: N_k, $k=1, \ldots, M$, $j=1, \ldots, N_k$.

Consider the set of M classes, $k=1, \ldots, M$ each with multidimensional normal distribution $f(\mathbf{r}/\mu_k)$ in the space of $\mathbf{r}_{jk}$, i. e. each class is characterized with an average vector $\boldsymbol{\mu}_k$ and a covariation matrix K_k.

With c_{kl} we denote the losses due to the case when the classifier makes decisions for availability of subject from the l-th class, while in reality there is a subject from the k-th class. The elements c_{kl} form the matrix C of the losses, $l=1, \ldots, M$.

We introduce decision surfaces S_{kl} for the classes k and l. The possibility to have error in unifold classification (of one vector $\mathbf{r}$) is:

$$p_{kl}=\int_{V_{kl}} f(\mathbf{r}/\mu_l)\, d\mathbf{r},$$

where V_{kl} is the volume, in which (through S_{kl}) the k-th class is defined. The average value of c_{kl} losses from all combination (k, l) and for multifold repeated classification (for many vectors $\mathbf{r}$) is called risk function R and is obtained from

$$R=\sum_{k=1}^{M} \int_{V_{kl}} \sum_{l=1}^{M} p_k c_{kl} f(\mathbf{r}/\mu_l)\, d\mathbf{r},$$

where p_k is apriori probability of the k-th class.

Usually it is assumed that $c_{kk}=0$ and $c_{kl}=\text{idem}=c$, i. e. no loss of correct classification occurs and in incorrect classification all the classes are assumed to be of equal weight with regard to the losses. Under this simplifying condition ensuing from the principle of maximum similarity it follows that the equations for s_{kl} are:

$$(1) \qquad S_{kl}: ln \frac{p_k}{p_l}+l_n \frac{|K_l|}{|K_k|} - \frac{1}{2}[(\mathbf{r}-\mu_k)' K_k^{-1} (\mathbf{r}-\mu_k)-(\mathbf{r}-\mu_l')K_l^{-1}(\mathbf{r}-\mu_l)]=0.$$

Equation (1) ensures the minimum R value.

Appendix 2

Variation coefficient of the Fourier series coefficients under linear approximation of discrete SRS

The real SRS are obtained in discrete shape: $\mathrm{r}(\lambda_i)$, $i=1, \ldots, m$. Under a large channel number, for example, $m=32$, the linear approximation is acceptably correct. In this case the coefficients a_k of the basic orthogonal functions $\sin \frac{k2\pi\lambda}{T}$ are expressed with [21]

$$a_k = -\frac{1}{\pi} \sum_{i=1}^{m} \frac{\beta_i}{k^2} \left(\cos \frac{k2\pi}{T} \lambda_i - \cos \frac{k2\pi}{T} \lambda_{i-1} \right) \tag{1}$$

$$= \frac{2 \sin \frac{k\pi}{T} \Delta\lambda}{\pi k^2 \Delta\lambda} \sum_{i=1}^{m} (r_i - r_{i-1}) \sin \left[\frac{k2\pi}{T} (\lambda_i + \lambda_{i-1})/2 \right].$$

We assume that r_i are normally distributed random values of dispersion $\sigma_i^2 = q^2 \mu_i^2$ where $q \ll 1$, for example, 0,03. Such an assumption of rigid proportion between σ and the average vector μ we introduce for convenience [18, 20] of the comparative analysis. We assume also that $r(\lambda)$ is a periodic function of period T. In reality this is not true, and in order to apply the Fourier series of $r(\lambda)$, we have to assume that $r(\lambda)$ performs a jump, for example, in λ_m, and attains the value of r_{λ_1}. This assumption in principle does not introduce difficulties in the classification, but requires the introduction of additional terms in the transformation to describe the nonlinearity of the jump. The periodicity of the function thus defined makes the coefficients a_k independent between themselves, for example, [9]. Then the mean square deviation of $\bar{a}_k$ from (1) equals to

$$\sigma_k = q \frac{2 \sin \frac{k\pi}{T} \Delta\lambda}{\pi k^2 \Delta\lambda} \sqrt{\sum_{i=1}^{m} \left\{ (\mu_i^2 + \mu_{i-1}^2) \sin^2 \left[\frac{k2\pi}{T} \frac{\lambda_i + \lambda_{i-1}}{2} \right] \right\}}. \tag{2}$$

The coefficient of variation of a_k is respectively equal to

$$V_k = \frac{\sigma_k}{\mu_k} = q \frac{\sqrt{\sum_{i=1}^{m} \left[(\mu_i^2 + \mu_{i-1}^2) \sin^2 \frac{k\pi}{T} (\lambda_i + \lambda_{i-1}) \right]}}{\sum_{i=1}^{m}{}' (\mu_i - \mu_{i-1}) \sin \frac{k\pi}{T} (\lambda_i + \lambda_{i-1})}. \tag{3}$$

For comparison we may use the variation coefficient of r_i

$$V_i = \sigma_i / \mu_i = q. \tag{4}$$

The comparison between (3) and (4) shows that it is possible even for small k values, i. e. for main harmonics, to obtain $V_k > 1$, because the expression in the denominator of (3) is a sum of terms of different signs. For example, for the discrete series of 32 values (linearly approximated) for $r(\lambda)$: 53, 51, 48, 46, 43, 42, 41, 41, 40, 40, 41, 41, 42, 38, 36, 28, 29, 48, 53, 53, 98, 85, 65, 50, 38, 33, 35, 30, 27, 45, 53 under $k=5$ we obtain: $V_k = V_5 \approx 8{,}8\ q$.

When the discrete Fourier transformation is applied to obtain V_k the well-known relationship between the Fourier series coefficients and its discrete version has to be applied [21].

Appendix 3

I. Autocorrelative function (for example [22])

$$K(\tau_j)=\sum_{i=1}^{m}[r(\lambda_i)-\bar{r}(\lambda)]\,[r(\lambda_i+\tau_j)-\bar{r}(\lambda)],$$

where

$$\bar{r}(\lambda_i)=\sum_{i=1}^{m} r(\lambda_i)/m, \quad j=0, 1, 2, \ldots, m-1, \tau_j=(\lambda_i-\lambda_{i-1})\,j=\Delta\lambda\,.\,j.$$

II. Power autocorrelative function [8, 18, 23]

$$C^{(n)}(\tau_j)=\sum_{i=1}^{m}|r(\lambda_i)-r(\lambda_i+\tau_j)|^n$$

n is given by the user, for example, $n=0{,}5\,;\ 1\,;\ 2\,;\ldots$ (under $n=2$, the Kolmogorov function is obtained [22])

$j=1, \ldots, m/2$ for m even,

$j=1, \ldots, (m+1)/2$ for m odd,

τ_j as for $K(\tau_j)$.

III. Integral (mean arithmetic) transformation [24]

$$I(\lambda_l)=\frac{1}{l}\sum_{j=1}^{l} r(\lambda_j), \quad l=1, \ldots, m.$$

IV. Combined transformation [24]

$$L(\tau_j)=C_j\,.\,I[r(\lambda)]=\sum_{i=1}^{m}|I(\lambda_i)-I(\lambda_i+\tau_j)|^n,$$

$j=1, \ldots, m/2$ for m even,

$j=1, \ldots, (m+1)/2$ for m odd.

Transformations I, II and IV are invariant with respect to an additive constant, i. e. they are filter of systematic, additive and apriori unknown errors.

All the transformations shown are irreversible. The ratios between the coefficients of variation of I, II and untransformed SRS are obtained in [18, 20] under the following limiting conditions: a) $\sigma_i=q\,.\,r_i$, $q\ll 1$; b) random values r_i and r_j are interindependent; c) the differences between the uniform components of the mean vectors r_k and r_l of two classes are small and are measured with $\theta\ll 1$. Under these conditions, from [18, 20] it follows that the variation coefficient V_c of $C^{(n)}(\tau_j)$ is minimum at $n=1$ (n-integer) and it follows from [23] that $V_C^{(n=1)}$ is smaller than V_k and with $m>8$ also from $V_r\,.\,V_r$ is the

variation coefficient of untransformed SRS. The last estimate: $m>8$ is approximative.

The upper ratios are deduced under conditions that differ from reality (for example, the covariation matrices are not diagonal). They may serve as orientation in the effectiveness evaluation of the transformations exposed.

In [24] the evaluation of transformations III and IV is performed which exhibits their effectiveness with reference to the reduction of the risk function R value. The evaluation is performed under limiting conditions similar to the above-mentioned.

Appendix 4

Enthropic and divergence transformations

I. Enthropic transformation [9, 12].

The matrix A of the linear transformation $\varkappa=A\mathbf{r}$ is determined so as to minimize the enthropy

$$H_j=-\int_{(\mathbf{r})} p(\mathbf{r}/\omega_j)\ln p(\mathbf{r}/\omega_j)d\mathbf{r},\quad j=1,\ldots,M,$$

where the integration is in the $\mathbf{r}$ space of SRS, ω_j is denomination of the j-th class, and $p(\mathbf{r}/\omega_j)$ is density of probability distribution for the j-th class. Maximum uniformity (structuring) of set $\{p(\mathbf{r}/\omega_j)\}$ corresponds to $H_{\min}$. This corresponds to minimization of the dispersion in various distributions and may be expected to improve the identification of the classes.

Under equal covariation matrices K of the M-th classes, A is obtained as a matrix of eigen vectors.

II. Divergence transformation [9, 12].

The matrix A is determined for the linear transformation $\varkappa=A\mathbf{r}$, so as to maximize the divergence (difference in information) between the j-th and k-th classes

$$I_{jk}=\int_{(\mathbf{r})}[p_j(\mathbf{r})-p_k'(\mathbf{r})]\ln\frac{p_j(\mathbf{r})}{p_k(\mathbf{r})}d\mathbf{r}.$$

Under equal covariation matrices $K_j=K_k$ the maximum divergence thus obtained equals the risk function for j and k classess under the condition that $c_{jk}=c_{kj}$ (see Appendix 2). Therefore, it is assumed that I_{jk} here may act as a measure of distinguishing between classes j and k.

In the real case $K_j\neq K_k$ and $\mu_j\neq\mu_k$. Therefore, the definition of A relates to large computing difficulties. Moreover, there is no general method to maximize I for a set of M classes so that secure reduction of R may be obtained.

References

1. Himmelblau, D. M. Process Analysis by Statistical Methods. Moscow, 1973 (Russ.).
2. Yanev, T., D. Mishev. Experimental planning for complex test site studies of spectral reflectance signatures of natural formations. — Seminar on Test Site Studies in Bulgaria, Asenovgrad, 1976.
3. Yanev, T., A. Stoimenov. Optimizing the multispectral volume on terrestrial studies of natural formations. — Compt. rend. Bulg. Acad. Sci., 31, 1978, 11.
4. Mishev, D., R. Kancheva. Test sites. — UN/FAO Remote Sensing Training Seminar. Sofia, 1981.
5. Mishev, D. Remote Sensing of the Earth. Sofia, 1981.

6. Milenkiy, A. Classification of Signal Under Indeterminancy. Moscow, 1975 (Russ.).
7. Mishev, D. Spectral reflective characteristics of natural formations and their application for remote sensing purposes. — Rem. sensing of the earth, 1980, 1.
8. Yanev, T., G. Astardgiyan, Ch. Nachev. Feature set yield and decision-making in analysing monodimentional objects. Large systems of information and control. — 4th Polish-Bulgarian Seminar, Varna, 24-25 Oct., 1973.
9. Tou, J., R. Gonzalez. Pattern Recognition Principles. Moscow, 1978 (Russ.).
10. Mishev, D., T. Yanev. Separation of mixture from spectral reflective characteristics within a pixel. — University Annual. Technical Physics, 12, 1984, 1.
11. Classification and Clustering. Edit. Ryzin van J. Moscow, 1980 (Russ.).
12. Young, T., Th. Calvert. Classification, Estimation and Pattern Recognition. New York, 1974.
13. Patrick, E. Fundamentals of Pattern Recognition. Moscow, 1980 (Russ.)
14. Fu, K. S., D. A. Langrebe, T. L. Phillips. Informational Processing of Agricultural Data Obtained through Distance Measurements. — TIEP, 1968, MX.
15. Kondratiev, I., A. Grigoriev, O. Pokrovski. Informational Content of Remote Sensing Data on Environmental and Natural Resources Parameters. Leningrad, 1975.
16. Remote Multispectral Sensing in Agriculture, Laboratory for Agricultural Remote Sensing. — Annual Rep., Lafayette, Indiana, 1970.
17. Duda, R., P. Hart. Pattern Classification and Scene Analysis. Moscow, 1976. (Russ.)
18. Yanev, T., D. Mishev. Discriminant analysis of natural formation reflective characteristics by a minimal number of wavelengths. — XVIII COSPAR Mtg., Varna 29 May—7 June, 1975.
19. Yanev, T. Optimization of a parallelepiped discriminant function at a multidimensional analysis. — Space Res. in Bulgaria, 1978, 1.
20. Yanev, T., D. Mishev. Multidimensional classification analysis of spectral reflective characteristics obtained by aircraft, satellites and earth surveys. — XIX COSPAR, Philadelphia, June 1976.
21. Hamming, R. Numerical Methods for Scientists and Engineers. Sofia, 1974 (Bulg.).
22. Romanenko, A., G. Sergeev. Problems of the applied analysis of random processes. — Sov. Radio, Moscow, 1968 (Russ.).
23. Yanev, T. Power autocorrelative function. — Space Res. in Bulg., 1978, 1.
24. Mishev, D., T. Yanev. Comparison of discriminating possibilities of some transformations of spectral reflective characteristics of natural formations. — Compt. rend. Bulg. Acad. Sci., 31, 1978, 5.
25. Yanev, T., D. Mishev. Mathematical-statistical methods for object classification through spectral reflective characteristics. — UN/FAO Regional Training Seminar on Remote Sensing Application for Land Resources. 16-26 Sept., 1981, Sofia.
26. Yanev, T., D. Mishev. Program package for classification of spectral reflectance signatures. — First Bulgarian-Soviet Seminar on the Results from Bulgaria-1300 Project. Sofia, December, 1981.
27. Minskiy, D. E., A. M. Chizhevskiy. Fast Classification of Multizonal Imagery by Bayes. — Remote Sensing of the Earth. 1982, 1.
28. Yanev, T., D. Mishev. Methodics for the analysis of the spectral characteristics. — Mtg. of the Working Group of the Socialist Countries on Remote Sensing of the Earth with Air- and Space-Borne Techniques within the Framework of the Intercosmos Program. 25-30 May, Smolenište, Czechoslovakia, 1981.

Математико-статистические методы классификации спектральными отражательными характеристиками

Т. Янев, Д. Мишев

(Р е з ю м е)

Проведен сравнительный анализ существующих методов классификации спектральными отражательными характеристиками (СОХ) природных образований. Предложены методика и блоковая структура пакета программ для классификации СОХ и актуализации параметров классификатора.

Методика основана на подходе Бейеса в режиме с учителем и на кластерном анализе в режиме без учителя. Выполняются предварительные преобразования СОХ с целью уменьшения функции риска. Определяется минимальное число каналов прибора получения СОХ, достаточных в данном тематическом классификаторе для достижения заданной функции риска.